CDF Note 6312
April 25, 2004

Isolated prompt diphoton central-central cross-section measurement at CDF Run II

Robert Blair,Raymond Culbertson,Joey Huston, Steve Kuhlmann, Yanwen Liu, Xin Wu

Abstract

A measurement of the rate of prompt diphoton production in $\overline{p}p$ collisions at $\sqrt{s} = 1.96$TeV using the CDF II detector is presented. The background from non-prompt sources is estimated using a statistical method based on the difference in EM showers initiated by photons and background. The results are compared to a next-to-leading order calculation.

Contents

List of Tables

List of Figures

1 Motivation

The $H \rightarrow \gamma\gamma$ decay mode is a useful channel for the standard model (SM) Higgs boson searches in the low mass region ($M_H < 130$ GeV) at the forth coming LHC. In many models involving physics beyond the standard model, cascade decays of heavy new particles generate $\gamma\gamma$ signature. Some examples are supersymmetry with a light gravitino, radiative decays to a higgsino-LSP and models with large symmetry groups. The QCD production of prompt photon pairs with large invariant mass is the irreducible background to these searches. The rate is huge and requires to be understood and quantitatively evaluated prior to any of the possible discoveries. In hadronic collider environment like LHC, prompt photon signals are contaminated by the production of neutral mesons which decay to multiple collinear photons. The experience of classifying background of neutral meson source with Tevatron data is very important.

The process is interesting on its own right. The 4-momentum of particles in the di-photon final state can be precisely determined due to the fine resolution of EM calorimeter. The imbalance in the transverse momentum of the two photons provides a clear probe of the transverse momentum of the colliding partons. At collider energies, most of the transverse momentum of the incoming partons can be attributed to multiple soft gluon emissions prior to the collision, of which the effect to di-photon production can be resummed by Collins-Soper-Sterman (CSS) formalism. The di-photon data can be used to test the resummation formalisms.

2 Trigger

We used events collected by $DI\_PHOTON\_12\_ISO$ trigger, which requires two isolated em clusters with Et above 10 GeV at L2, two isolated EM objects with Et above 12 GeV at L3. See Table 1 for the detailed description of the trigger path.

2.1 Trigger efficiency

Different versions of reconstruction were running at L3 and offline, resulting in slightly different em quantities. For example, photon variables were calculated assuming zVertex = 0 at L3, causing smearing between L3 and offline Et. The difference between

L1 :
single trigger tower Et>8GeV HadEm < 0.125 [1] [2]
L2 :
Two high em pass Em Clusters(clustering with trigger-tower segmentation [2])
HadEm < 0.125
Isolation < 3 GeV .or. Isofraction <0.15
Et > 10GeV
L3 :
Two em objects
average CES χ^2 <20.
Et > 12 GeV
HadEm < 0.055+0.00045*E
Isolation < 2.GeV .or. Isofraction < 0.1

Table 1: diphoton trigger specification. Note that L2 and L3 quantities are formed with zVertex = 0.

L3 and offline might have introduced some inefficiency to our L3 trigger. L2 uses different clustering algorithm, and isolation definition, which might have caused some more inefficiency. We used events from inclusive photon trigger(PHOTON_25_ISO) to evaluate the trigger efficiency. For each event that passed the inclusive single photon trigger, we count how often the diphoton trigger bit was set if there are two isolated photon candidates found in the event offline. In figure 1, we plotted this probability as function of Et of the next-to-leading photon candidate in the event.Since PHOTON_25_ISO trigger cuts are the same as the diphoton trigger does per each leg, except for the higher Et threshold, this probability can be interpreted as the probability of the next-to-leading leg satisfying the diphoton trigger requirement. The ideal way to measure the trigger efficiency is to use a pure signal sample. Here we used a mixture of signal and background to do the job, where the background is mainly from neutral mesons such as π^0 which decay to multi-$\gamma's$. Since the efficiency at the high Et plateau we obtained(0.997) is close to 100%, the systematic uncertainty of this study is limited to one percent level. In fact, we loosened the isolation cut and extra CES cluster energy (both strip and wire view) to 2 GeV for the denominator to include more background, and found the trigger efficiency remained the same(0.991 for the loose cuts).We cover this by adding 1% systematic uncertainty to the measurement. The statistics isn't too good in the turn-on region, we varied the fitted parameters by the error from fitting, and found trigger efficiency curve can move around by 1%. In the end, we included 3% of uncertainty to the analysis from trigger efficiency.

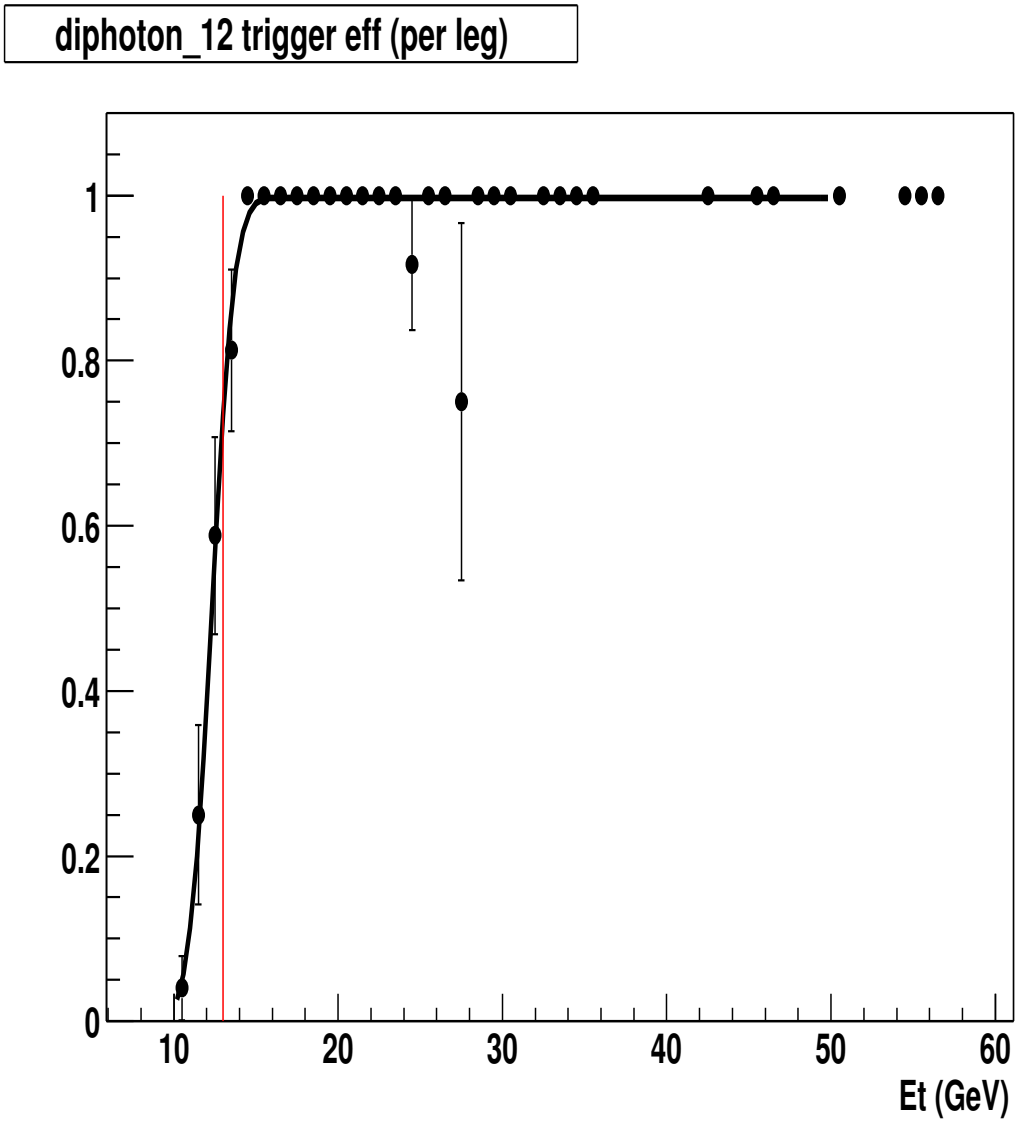

Figure 1: DI_PHOTON_12ISO efficiency vs the next-to-leading em object Et (GeV), parameterized as $p0 * Erfc(p1 * (p2 - Et))$ (fitted parameters are : p0 = 4.98695e-01 ± 6.56155e-03, p1= 6.49414e-01 ± 1.14311e-01, p2 =1.23154e+01 ± 2.06161e-01) to unweight data points. Numerator : diphoton_12 trigger bit. Denominator : photon_25_iso trigger bit and two isolated em objects found in CEM. See text for details. The red line is at 13. GeV, where we placed the Et cut at offline in this analysis.

central and |rapidity| < 0.9
|zVertex| <60 cm
$E_T^{\gamma 1}$ > 14 GeV and $E_T^{\gamma 2}$ >13 GeV
Isolation in 0.4 cone < 1 GeV.
No 3D track pointing to the em cluster
|Xces|<17.5 cm 14 cm <|Zces| <217 cm
no extra ces cluster above 1 GeV
average ces chisq < 20
HadEm < 0.055 + 0.00045*E

Table 2: offline cuts (see later in the note for the reason of the asymmetric Et cuts.)

3 Event selection

The offline cuts are the same as in Run I, except for the Et threshold. Run I diphoton analysis [3] had 10 GeV as the Et threshold in trigger, 12 GeV at offline to avoid trigger inefficiency caused by Et smearing. In Run II we have 12 GeV in the trigger, and decided on 13 GeV at offline to void the region where the trigger is very inefficient. Further, we raise the Et cut on the leading photon to 14 GeV to make the Et cuts asymmetric to void the instability of NLO predictions, see later in this note. We listed the cuts in Table 2, and evaluated the cut efficiencies in succeeding sections.

3.1 Detector acceptance and reconstruction efficiency

Diphoton Pythia Monte Carlo is used to measure the central detector acceptance(including reconstruction efficiency). With diphoton Monte Carlo events, we locate each of two prompt photons at generation level and check how often there is an offline em object matching it to evaluate the detector acceptance. [1] We plot the matching efficiency vs η, ϕ in Fig 2 and Fig 3 respectively. The central acceptance is calculated to be 0.880 per photon by averaging the matching efficiency vs η plot for η between -0.9 and 0.9 region. And, we find 0.650 of generated prompt photons have a matching em object at offline if to require the offline cluster to be located in CES fiducial volume, namely \|Xces\| <17.5 cm, 14cm < \|Zces\| < 217cm.

3.2 Isolation cut efficiency

The isolation in a 0.4 cone was required to be less than 1.0 GeV for each photon. In Fig. 4, we plotted the isolation distribution of prompt photons from diphoton Monte

[1] For the genp and offline matching, we require the offline em object to be within 0.4 cone in $\eta - \phi$plane around the genp photon, and the energy difference to be within 50%

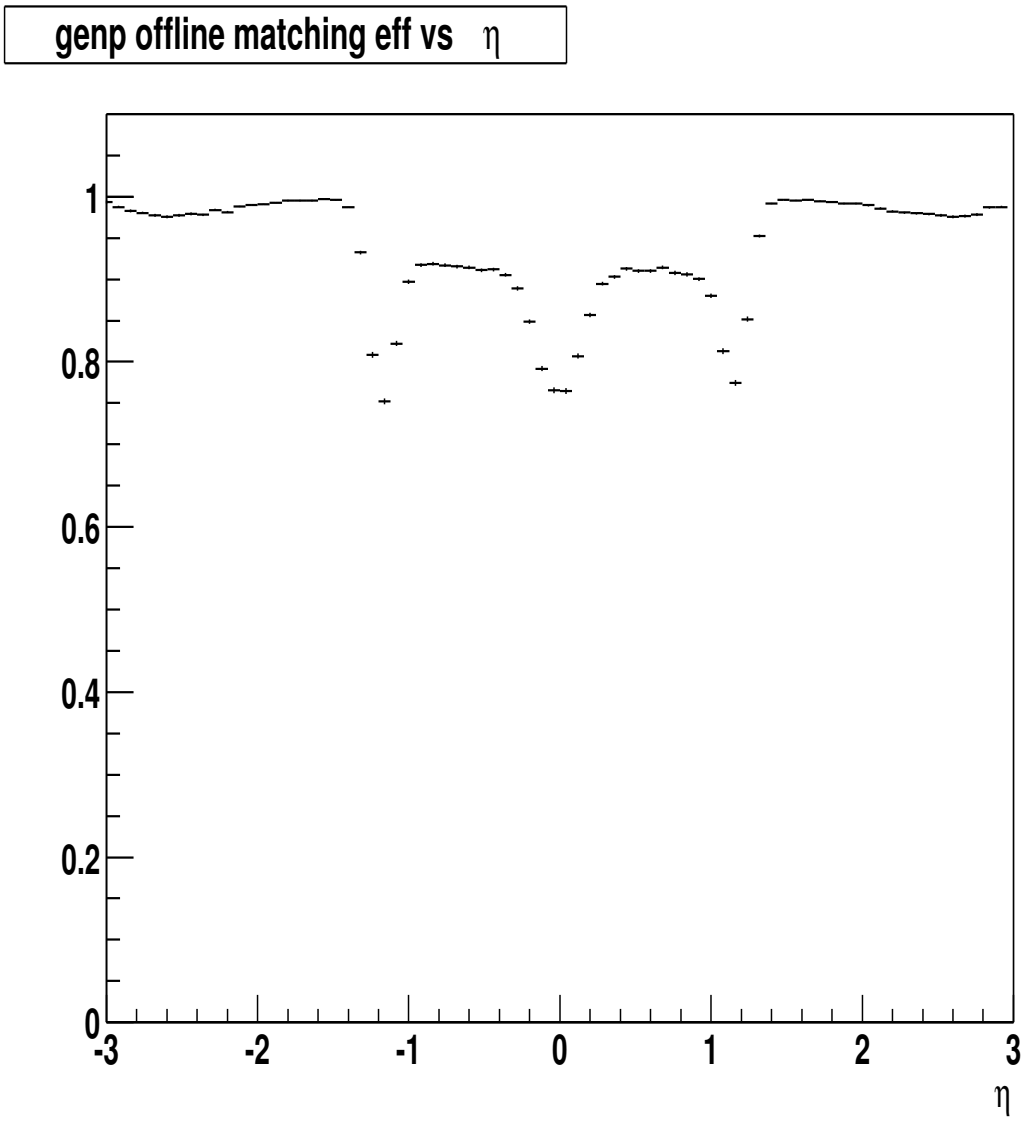

Figure 2: genp photon matching to offline em object efficiency vs η from diphoton Pythia MC. Each event contributed two entries since there are two prompt photons in it.

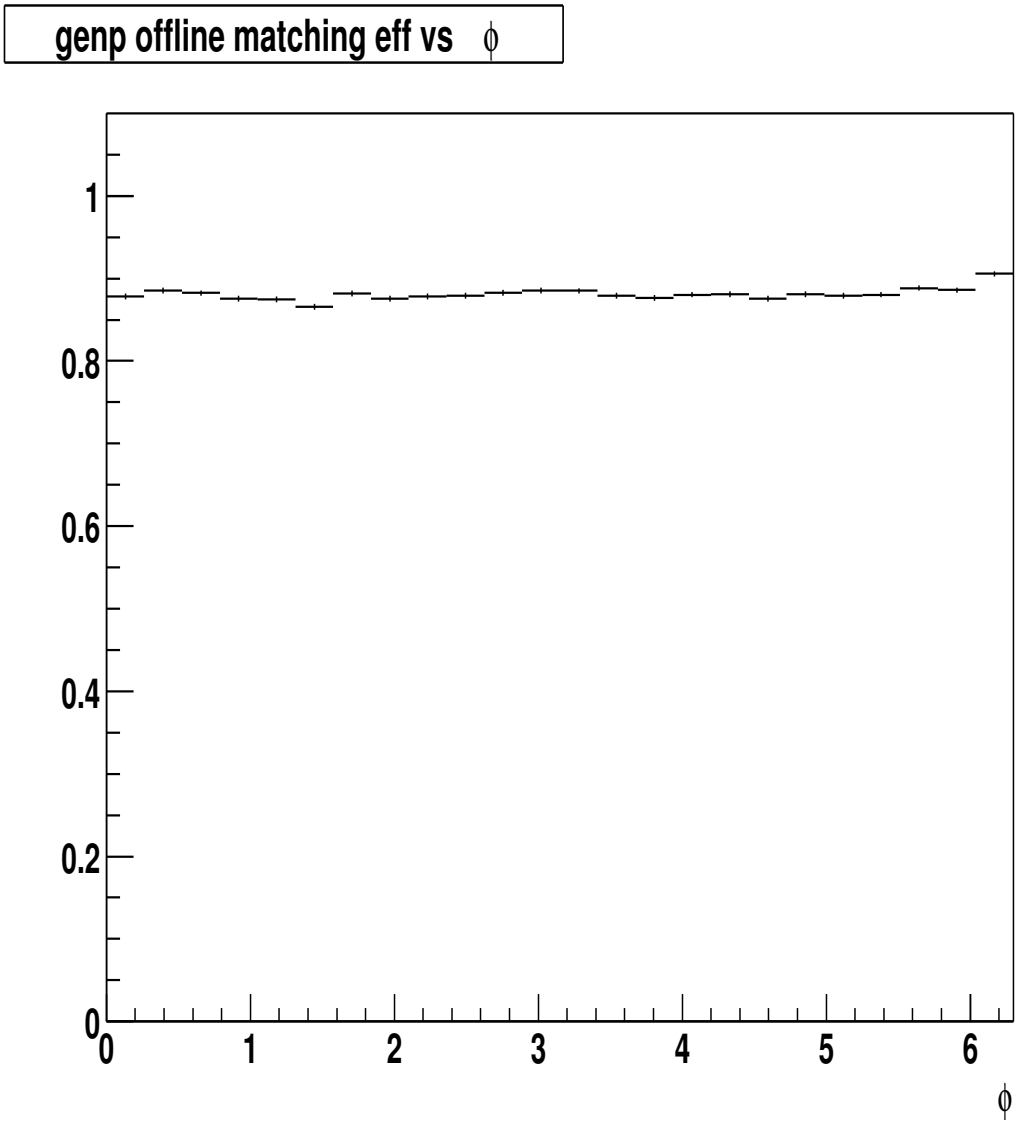

Figure 3: genp photon matching to offline em object efficiency vs ϕ, Each event contributed two entries since there are two prompt photons in it.

Carlo, where we found the efficiency of the 1.0GeV cut as 0.867 per photon.

As was done in Run I, we verified this efficiency by randomly placing virtual em clusters(flat in η, ϕ) on MB events, and calculating the isolation in the 0.4 cone of the virtual em cluster. We found 0.864 of the two-tower clusters having isolation below 1 GeV, 0.876 for three-tower clusters, which agreed with the number from MC to one percent : the 1% disagreement was taken as uncertainty on this efficiency.

3.3 No-track cut efficiency

We reject any em object with a track pointing to it. There are two inefficiency issues for this requirement : a good photon will be rejected if there is an underlying track pointing to it, or if the photon has converted in tracking volume to cause a reconstructed track. We plotted the track multiplicity of prompt photons in diphoton MC in Fig 5 . From that plot, the no-track cut efficiency is evaluated to be 0.862 per photon. It has been noted in [7] that the material amount was underestimated in the MC simulation. We corrected this efficiency by a factor of 0.97 as suggested and got 0.836. To convince ourselves that the MC got it right, we estimated the two efficiency issues separately in alternative ways. Firstly, the conversion probability is determined by material amount. We checked the OBSP quantities of the diphoton MC, and counted the conversion probability for photons in central to be 0.118. We obtain a conversion probability of 0.141 after the correction for additional material. Secondly, for the inefficiency caused by underlying tracks, we superimposed virtual em clusters on MB events, and extrapolated every track with Pt above 0.5GeV to the CES radius to check how often there would be at least one track associated with the virtual em cluster according to the em object cluster-track matching algorithm. We found from this study that 0.933 of the virtual em clusters would not be pointed at by any underlying track. In the end, the total efficiency is (1-0.141)*0.933 = 0.801, which differed from what we got from diphoton MC(0.836) by 4%. We use the 4% disagreement for the uncertainty on this efficiency.

3.4 No extra ces cluster above 1 GeV

We required that there should be no extra ces cluster above 1 GeV for both of the two photons. The efficiency of this cut was measured with diphoton MC to be 0.894. Since the CES simulation we have isn't a detailed geant simulation, we did a cross check. We took the unbiased z legs, cut tightly at E/p (require it to be between 0.9 and 1.1) to reduce the brem effects,and found 0.908± 0.008 of them passed the no extra CES cluster cut,which is in good agreement with what we got from diphoton

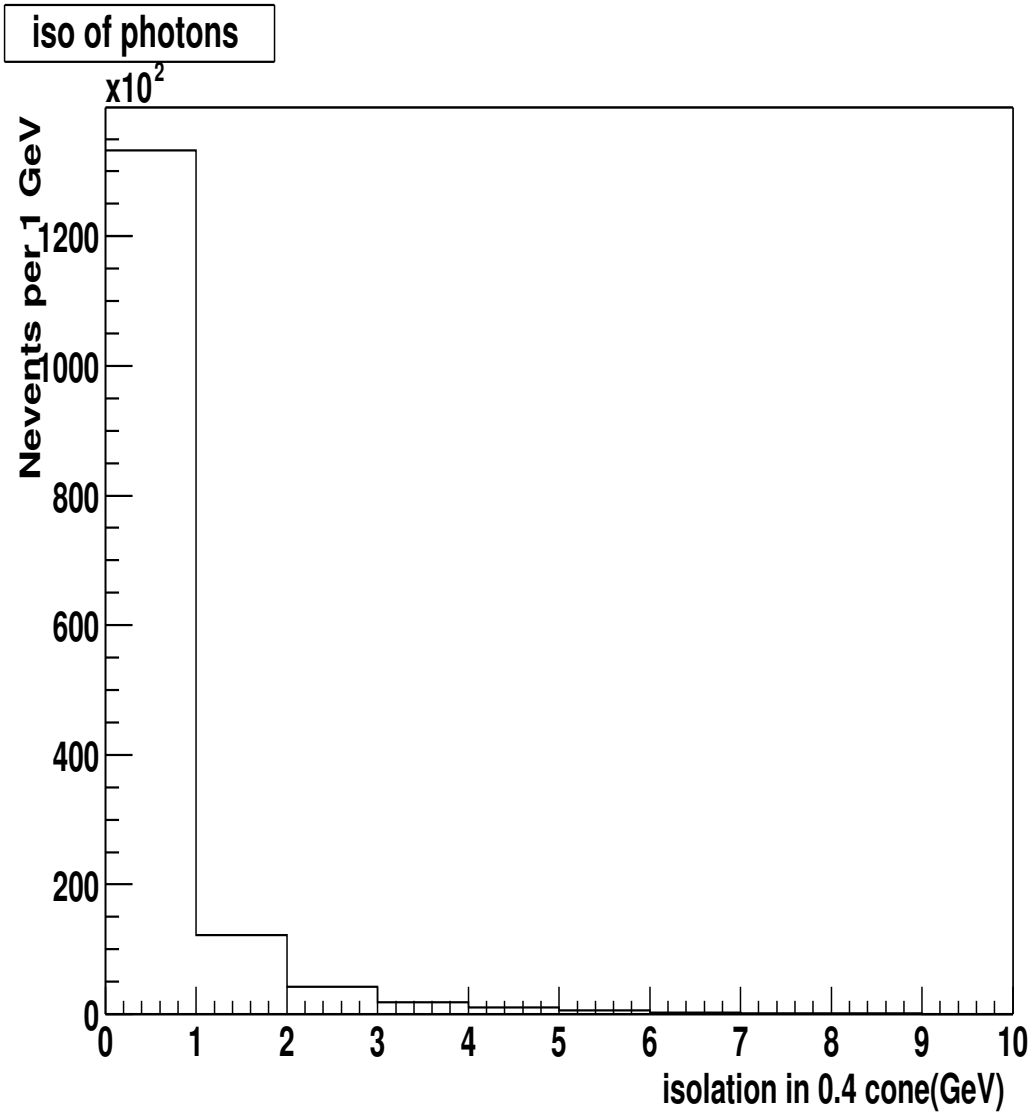

Figure 4: isolation in 0.4 cone (GeV) for prompt photons from Pythia diphoton MC.

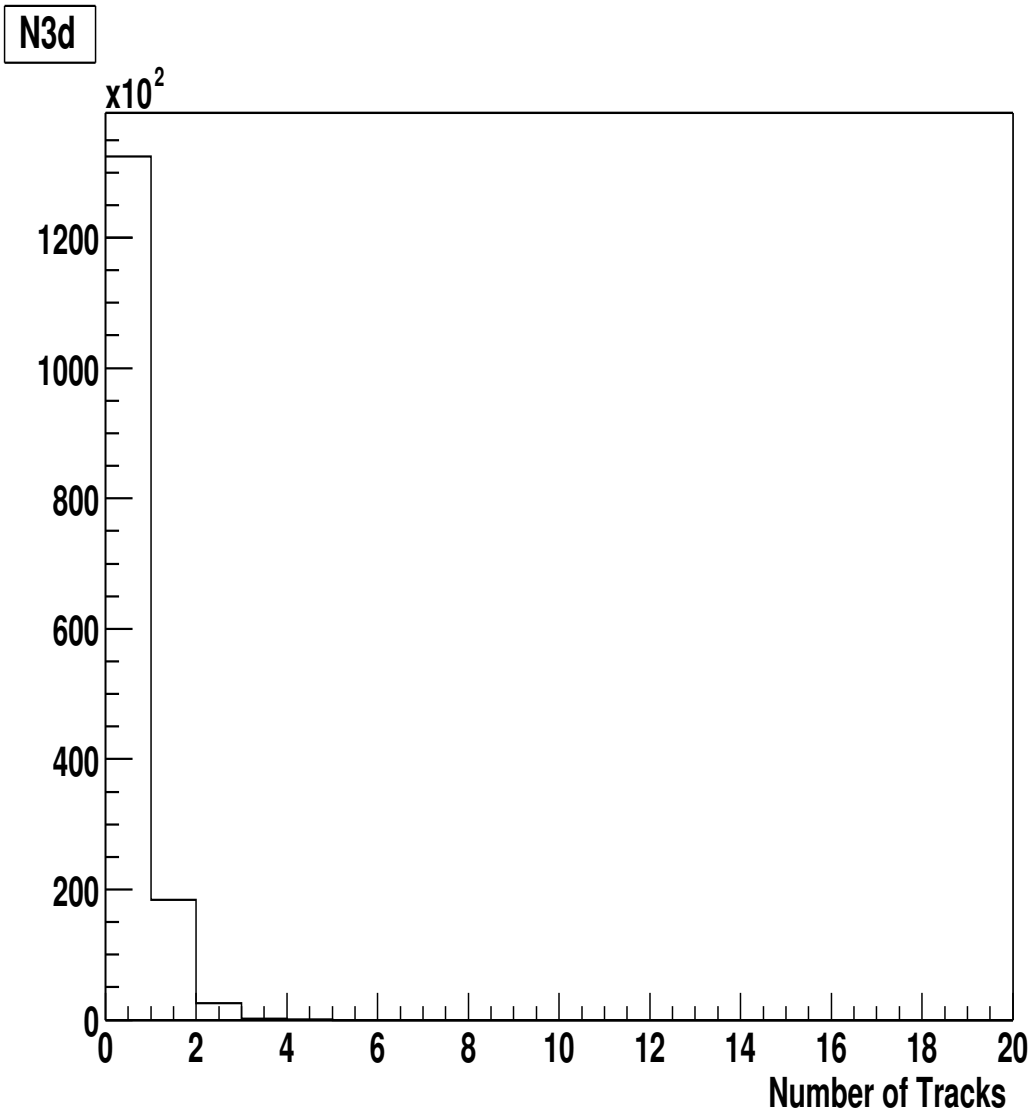

Figure 5: track multiplicity of prompt photons in diphoton MC.

MC. [2]

3.5 zVertex requirement

We required the zVertex between -60cm and 60cm. The efficiency of this cut has been measured in [8] to be 0.951. But for the diphoton analysis, both final state particles are track-less, and the vertex finding efficiency should be considered. The OBSP and reconstructed zVertex distributions of diphoton MC events are plotted in Fig 6. The vertex finding efficiency was found to be 0.922. To cross check with data : We found 628 diphoton candidates in the sample[3] if we release the zVertex cut, of which 34 were found with no vertices reconstructed. We verified that background events have higher vertex finding efficiency by varying the isolation cut to change the signal to background ratio. The vertexing efficiency from the 628 candidates (1-34/628 = 0.946) can be taken as the upper limit. We estimated 325.5 $\gamma\gamma$ events in the sample. The case that all the 34 candidates with no vertices are $\gamma\gamma$'s corresponds to the lowest vertexing efficiency : 1-34/325.5 = 0.896. In the end, we conclude that the $|zVertex|$ <60cm cut efficiency is 0.951*0.922 = 0.877. We cover both the lower and upper limit of vertexing efficiency by adding 3% uncertainty to the systematics.

3.6 CES chisq < 20. and HadEm < 0.055+0.00045*E cut efficiencies

Both of the cuts, CES chisq < 20 and HadEm < 0.055 + 0.00045*E, were assumed 100% efficient in the Run I analysis[3]. We checked these two cuts with unbiased z legs(E/p was required to be within the region [0.8,1.2] to reduce brem effect, only strip view was sampled for the chisq cut). Both cuts are about 99% efficient : 0.988 for the HadEm cut, 0.985 for the chisq cut.

3.7 Summary

We summarize the efficiency issues in Table 3.The over all acceptance for central diphoton events is 0.148. The uncertainties from the efficiencies introduced 11% to the sys. error of the analysis.

After these offline cuts, we found 893 diphoton candidates in our sample. See the invariant mass, Pt and $\Delta\Phi$ distributions in Fig 7, Fig 8 and Fig 9 respectively.

[2] As a student's exercise : I randomly placed virtual EM clusters on Min Bias events, and looked for CES clusters with energy above 1 GeV within geometry boundaries of the virtual clusters. For 100% (precision at order of 1e-03) of the cases, there wasn't any, which implies that underlying events weren't the inefficiency source.

[3] This is the diphoton sample when we've only 100 pb^{-1}

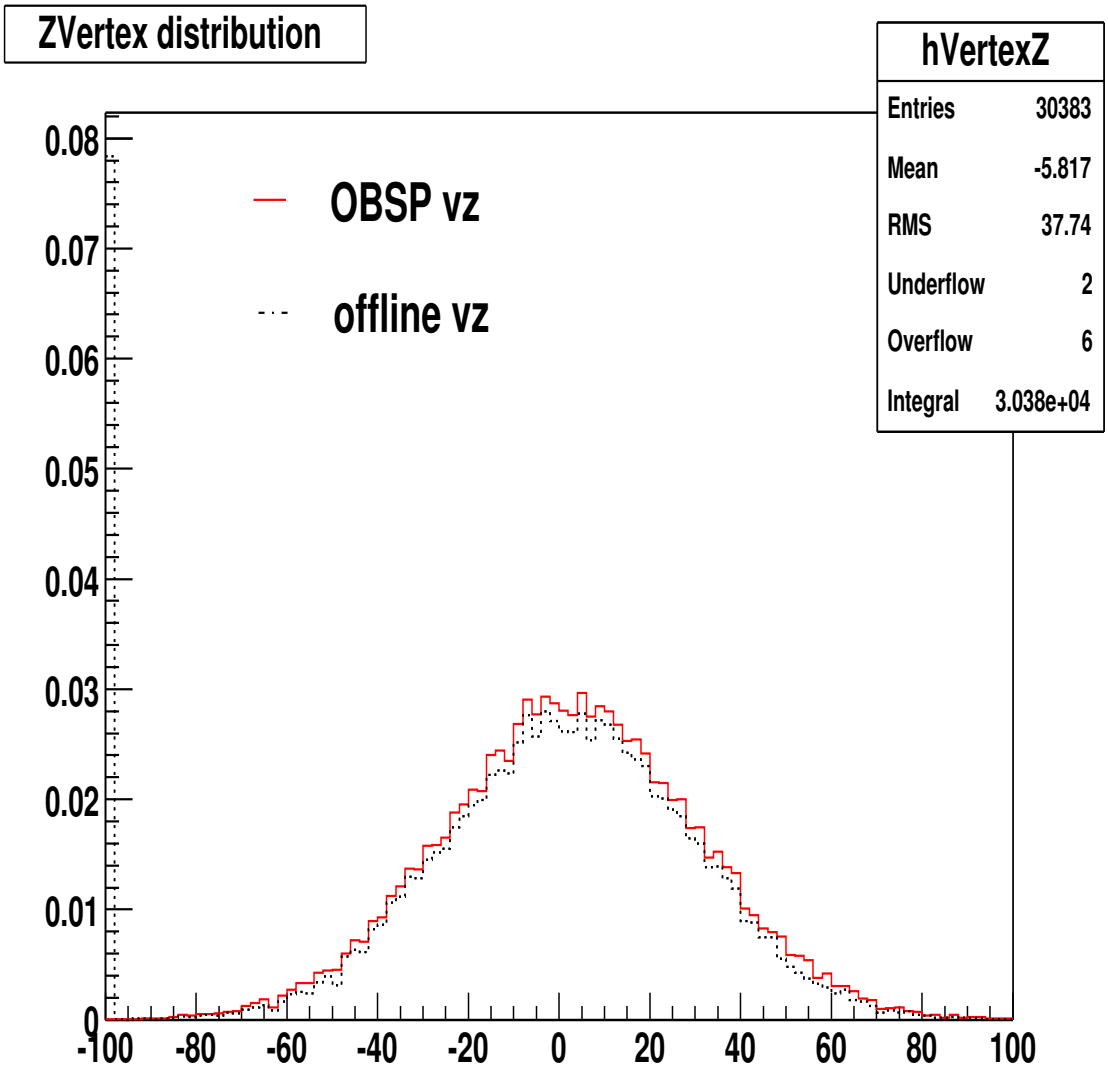

Figure 6: zVertex distribution of diphoton MC events : a number of events were found with no vertex reconstructed, and placed at the first bin (zv = -100.0)

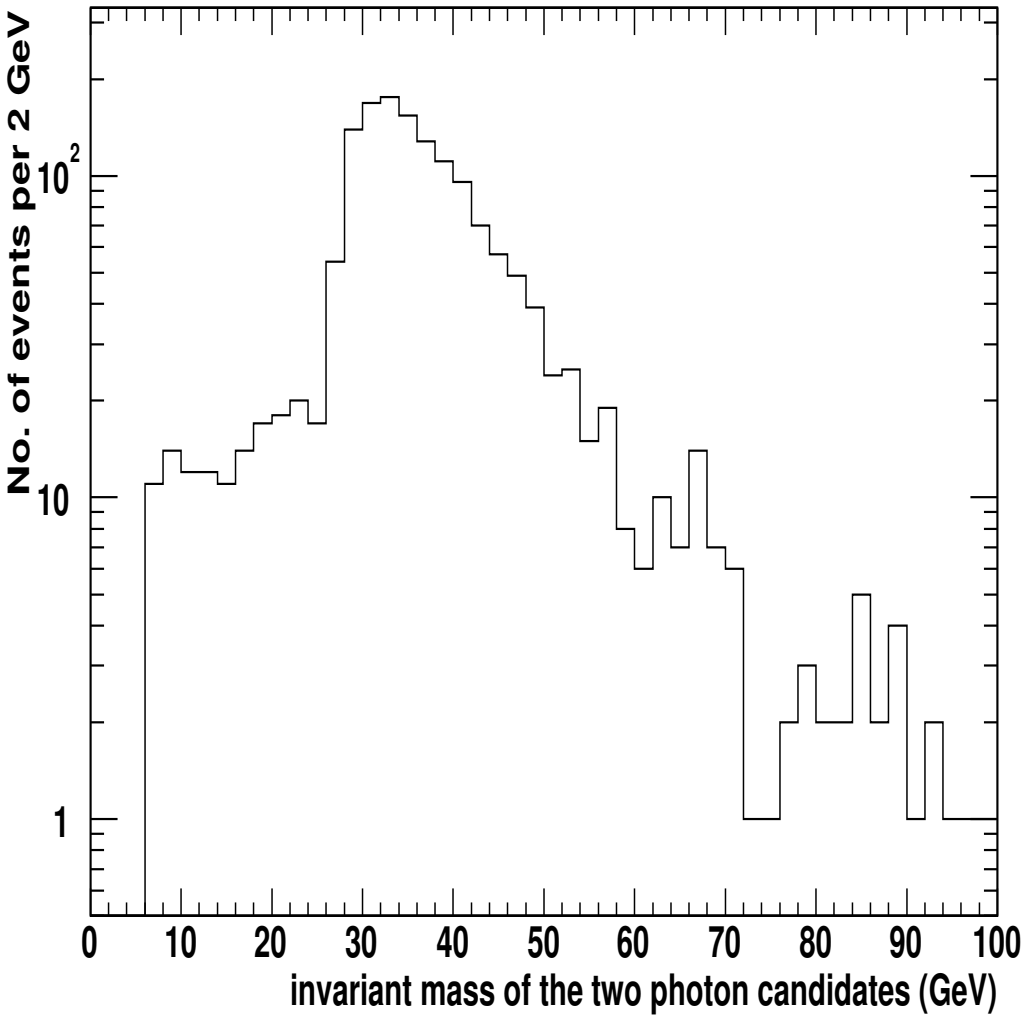

Figure 7: mass distribution (GeV) of the diphoton candidates

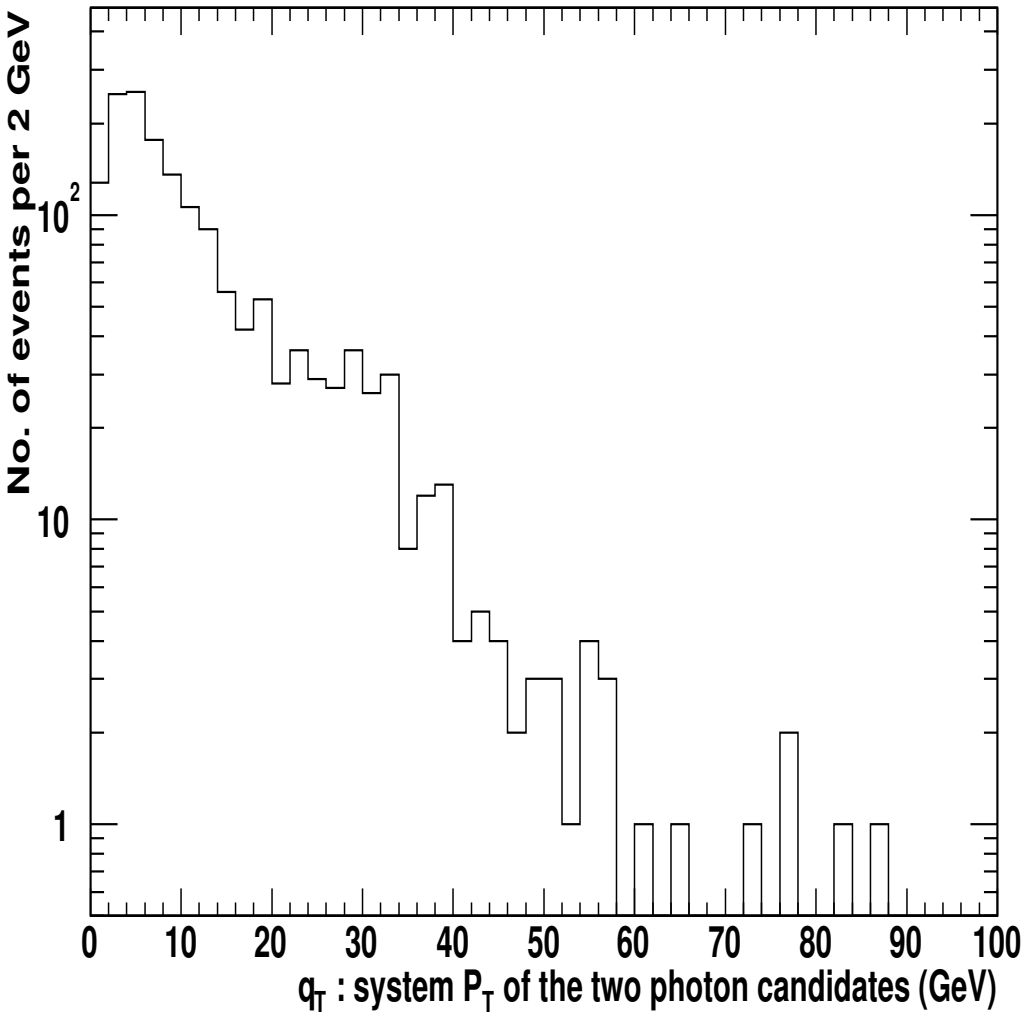

Figure 8: q_T (two-body system pT) distribution (GeV) of the diphoton candidates

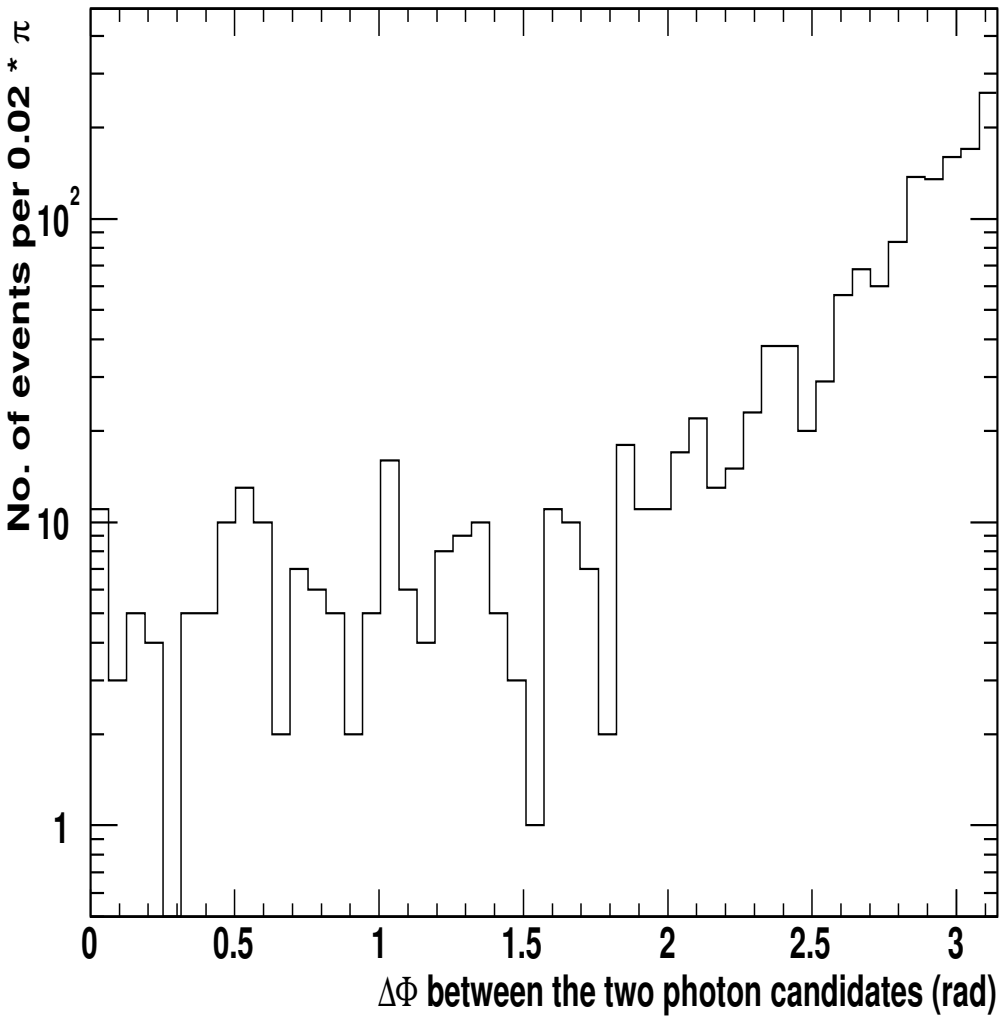

Figure 9: ϕ separation of the two em-objects in the diphoton candidates.

reconstruction efficiency and ces fiducial	0.650*0.650 = 0.423
iso in 0.4 cone < 1 GeV	0.867*0.867 = 0.751
No track pointing to the em cluster	0.836*0.836 = 0.699
No extra ces cluster above 1 GeV	0.894*0.894 = 0.799
CES chisq < 20	0.985
HadEm cut	0.988
|zVertex | < 60 cm	0.877
total	0.148

Table 3: efficiencies

4 Background subtraction

There is major background left in our candidates from neutral mesons such as π^0, η which decay to multi-γ's. We applied the same background subtraction as in Run I[3]: transverse profile (CES) method for Et<35 GeV, conversion (CPR) method for Et> 35 GeV. A detailed description of background subtraction for single photon can be found in [5]. The transverse profile (CES) method is vital for our analysis because it has an advantage at low Et where multiple photons from meson decays are more significantly separated at the CES radius. We re-calibrated and validate the constants (explicitly, $\chi^2 < 4/\chi^2 < 20$ fractions for both photons and neutral mesons.). Details can be found in [6]. In brief, we reconstructed η's that decayed to two photons residing in adjacent towers, by which we obtained a photon sample of 2-12 GeV in Et. We found from these photons that the $\chi^2 < 4$ fraction in Run II data (0.69±0.02) is lower than Run I prediction(0.75). We checked electrons from W and Z's (Et from 25 - 40 GeV), and found the fraction also about 0.05 lower than Run I prediction. We were then convinced that there was a -5% shift in the $\chi^2 < 4$ fraction for signal. The cause unknown. We fixed the background $\chi^2 < 4$ fraction by the "isolation test" : we adjusted it and compared the resulted background-subtracted isolation distribution of inclusive photon samples with that of unbiased z electron legs (biased with photon selection-like cuts for comparison.) We did this with both photon_10_iso and photon_25_iso events, and found a -0.05 shift in background $\chi^2 < 4$ fraction was needed to bring the subtracted isolation distribution in good agreement with that of z electron legs for both of the Et regions. We estimate the systematic uncertainty from background subtraction for this analysis as following : we use two sets of constants to apply the background subtraction with the diphoton candidates. One set is re-calibrated CES constants combined with CPR Run Ib constants, the other is Run I CES constants shifted by -0.03[4] combined with Run II re-calibrated CPR constants.

[4] 0.03 was the systematic uncertainty for the CES constants in Run Ib.

We double the difference in number of $\gamma - \gamma$ events obtained from subtractions with the two sets of constants, and add (in quadrature) the 10% uncertainty from Run I. Systematic uncertainty from background subtraction overall estimated this way was about 30% in [6].

After the subtraction, 426.02±58.97 events out of the 893 candidates were estimated as diphoton events.

So far, we've described how we get the numbers to determine the cross sections from data. In the next few sections, we'll introduce the theoretic predictions and compare the predicted differential cross sections with data. Of course, the differential cross section from data is obtained using

$$d\sigma/dX = Nevt/(\varepsilon_{total} * luminosity * binSize) \quad (1)$$

, where X can be any interested variable, such as invariant mass, q_T, and Nevt is the number of diphoton events in the bin, obtained from background subtraction technique mentioned earlier.

5 Cross section

We'll compare the data points with both DIPHOX[10] and ResBos[13]. DIPHOX is a computer program of fixed order calculation, which includes all contributing QCD processes consistently at next-to-leading order(NLO) (namely, $\alpha_{em}^2\alpha_s$) accuracy. ResBos can also predict the diphoton QCD production at NLO. In addition, it resums the effect of soft gluon emissions to all orders. However, we note that the fragmentation contribution in ResBos is effectively of LO. We'll discuss briefly some features of the two predictions. References by the theorists who did the work are strongly recommended for interested readers.

5.1 Divergences inside physical region of DIPHOX predictions and ResBos

As pointed out in [10], the observable q_T isn't infrared safe – it's sensitive to the emission of soft momenta. At the lowest order, the one fragmentation contribution with an isolation cut at E_T^{max} is discontinuous at $q_T = E_T^{max}$. For the LO one-fragmentation contribution, the isolation for the photon from fragmentation is just q_T in the DIPHOX isolation criteria implementation, implied by the conservation of transverse momentum conservation, thus the contribution to differential cross section takes a step function form. At NLO, the step-wise term is convoluted with the probability for emitting a soft and collinear gluon, and has a double logarithmic divergence. In a general analysis in [11], this class of singularities inside the physical

region arise whenever the observable in question has a non-smooth behavior in some order of perturbation theory. One solution would be to identify the problematic terms in each order of perturbation theory and resum them to all orders. We shall see that ResBos, re-summed the effect of the initial-state multiple soft-gluon emission with Collins-Soper-Sterman formalism, does predict a smooth q_T distribution.

Even infrared safe observables may have step-wise behavior at n-th perturbative order, and have singularity inside the physical region at the next order. In our case, we see a singular point at mass = 26 GeV if we cut the Et of both photons at 13 GeV– The prediction around m = 26 GeV isn't stable as we find by reducing the bin size of the DIPHOX mass curve. This divergence can be cured by applying asymmetric Et cuts [12] , for instance,

$$E_T^{\gamma 1} > 14GeV.and.E_T^{\gamma 2} > 13GeV. \tag{2}$$

, where $\gamma 1$ is the photon with higher E_T. We adopt the asymmetric Et cut stated above for a more reliable theoretic prediction. In Fig 10, we present the mass distribution predicted by DIPHOX, with symmetric Et cut. Note that the cross section drops to negative at mass = 26 GeV bin for the curve without $gg \to \gamma\gamma$ box contribution, when requiring both photons have Et > 13 GeV. With asymmetric Et cut, in Fig 11, the cross section prediction doesn't go below zero for either case.

5.2 ResBos and DIPHOX

Before going to data, We compare ResBos and DIPHOX. We apply asymmetric Et cut stated in Eq. (2) to both calculations.

We note the following :

- The invariant mass distributions agree pretty well for a vast mass region.Except for that, at very low mass, DIPHOX predicts much higher rates. The comparison can be found in Fig 12.

- As expected, the q_T distributions are very different. A comparison can be found in Fig 13. The ResBos curve is smooth for the overall region, while DIPHOX curve appears unstable at low q_T, due to the singularity we noted earlier. Another feature from the comparison is that at the high end, DIPHOX curve seems to receive some enhancement, while ResBos doesn't. This region corresponds mostly to the phase space where the two photons are about collinear. After some discussions with the authors of the two programs, the difference is understood : as we noted earlier, the fragmentation contribution in ResBos is effectively at LO. Since fragmentation to a photon is effectively of order α_{em}/α_s, some 2→3 processes like qg→gqγ, with the quark in the final state fragments to a

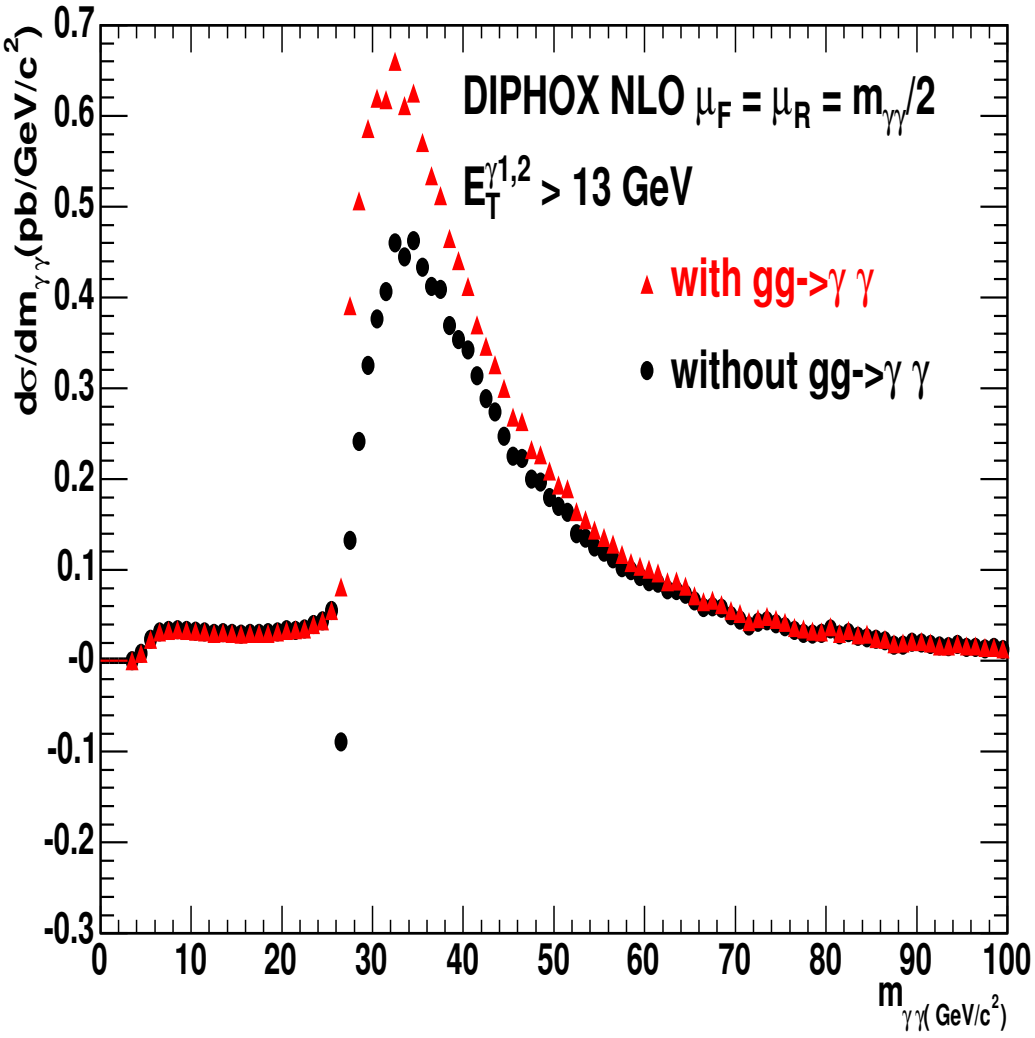

Figure 10: Invariant mass distributions by DIPHOX NLO predictions. The box contribution is negligible at high mass region. But there appears a singular point at the 26 GeV bin in the prediction without box contribution.

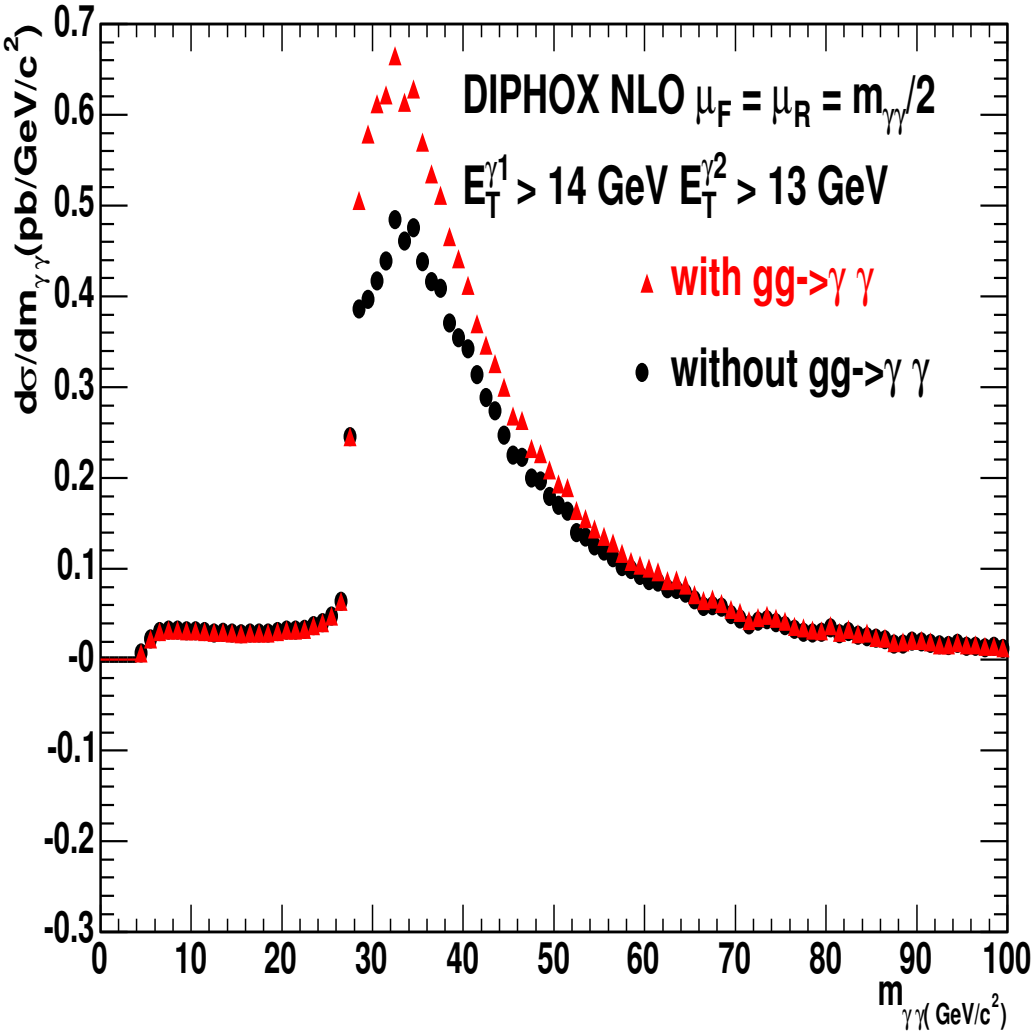

Figure 11: Invariant mass distributions by DIPHOX NLO predictions. No singular point on either of the two curves, with the asymmetric Et cut. We believe the prediction is more reliable with asymmetric cuts, and will adopt the asymmetric Et cut for data/theory comparisons.

second photon is effectively of order $\alpha_{em}^2 \alpha_s$. This contribution isn't in ResBos yet, which makes it underestimate the production rate at high q_T. In fact, the enhancement from fragmentation contributions has been observed before [14].

We'll check it further with the variable $\Delta\phi$, the azimuthal angle between the two photons.

- $\Delta\phi$: In Fig 14, for exactly the same reason explained above, ResBos underestimates the cross section at small $\Delta\phi$ due to the absence of 2→3 fragmentation contributions. In Fig 15, we only count $\phi_{\gamma\gamma} > \pi/2$ phase space, the q_T distributions look somewhat similar in shape between ResBos and DIPHOX.

5.3 Comparisons with data

We now start to compare the two predictions with the data. We include all the data up to September 2003 shutdown : run range 138425 - 168889, 207 pb^{-1}[5] in good runs, requiring offline COT,CAL, SMX and offline CAL,COT good run bits.

The mass distributions are compared in Fig. 16. The q_T distributions are compared in Fig. 17. The $\Delta\Phi$ between the two photons distributions are compared in Fig. 18. We notice the data points are in good agreement with both predictions in the mass distribution. In the q_T distribution, we see that in the low part, where the effect of soft gluon emissions is significant, the data points favor ResBos prediction. At large q_T the 2→3 fragmentation contribution becomes important, the data points seem to line up with DIPHOX curve better. Similar for $\Delta\Phi$. We must say that the statistical error still dominates the uncertainty of the measurement. The difference between data and either prediction isn't too outstanding. We binned the distributions of mass, qT and $\Delta\Phi$ from DIPHOX, ResBos and Pythia in the same way as we binned the data, and compared the production rate in each bin with data numerically in Table 4, 5 and 6.

In Fig. 19, we compare the mass distribution obtained from data with Pythia MC. The data points are significantly above the Pythia curve. We scale the Pythia curve up by a factor of 2.21 and overlay on data points in Fig. 20. We conclude that they appear pretty close in shape.

There are still interesting things to look at. As described in [14], the NLO fragmentation populates small mass and high q_T regions, which looks like an opening of phase space in $\Delta\Phi > \pi/2$. It's instructive to divide DIPHOX predictions into two regions : $\Delta\Phi > \pi/2$ and $\Delta\Phi < \pi/2$. We do so, and compare with data. In order to illustrate the higher order effects, we put on Pythia curves as references. We compared mass and q_T in this fashion in Fig. 21 and Fig. 22 respectively.

[5] 207 is the number after having applied the factor of 1.019.

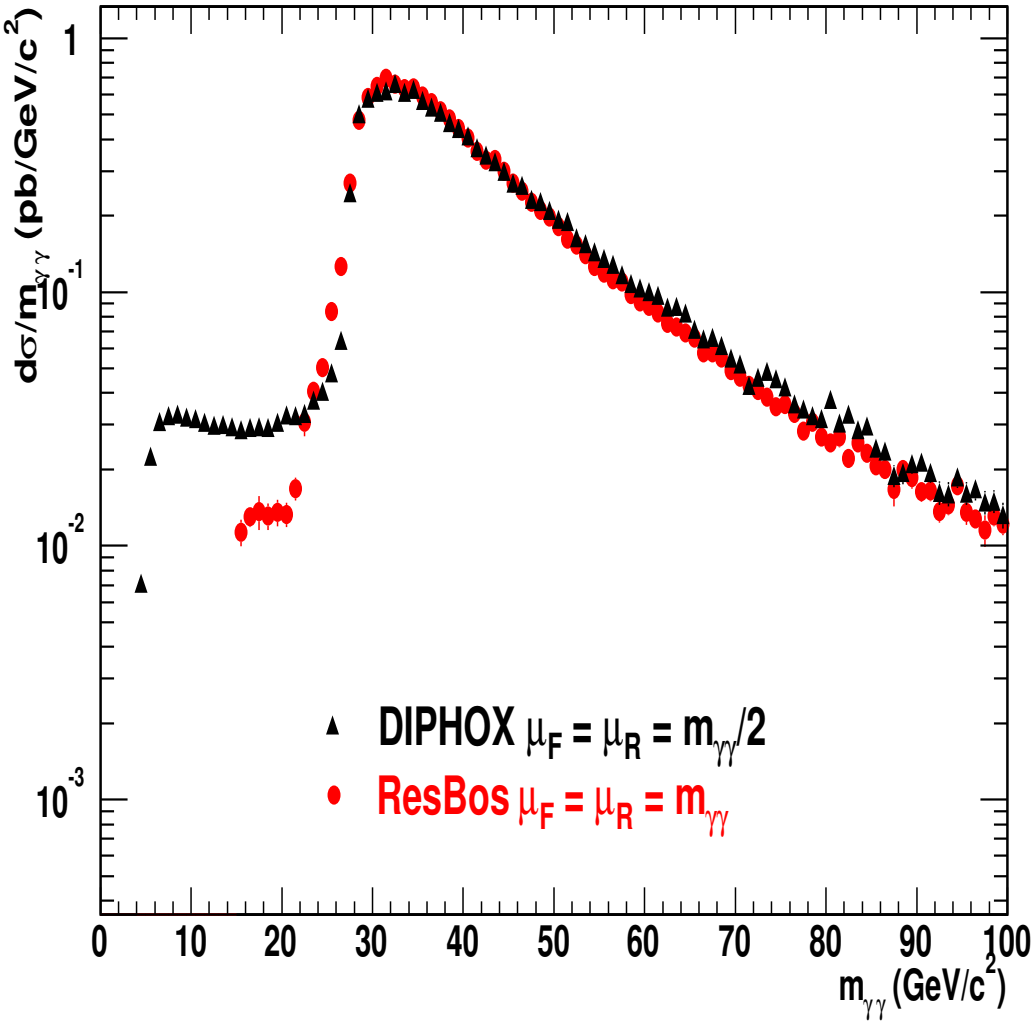

Figure 12: Invariant mass distributions from DIPHOX and ResBos.

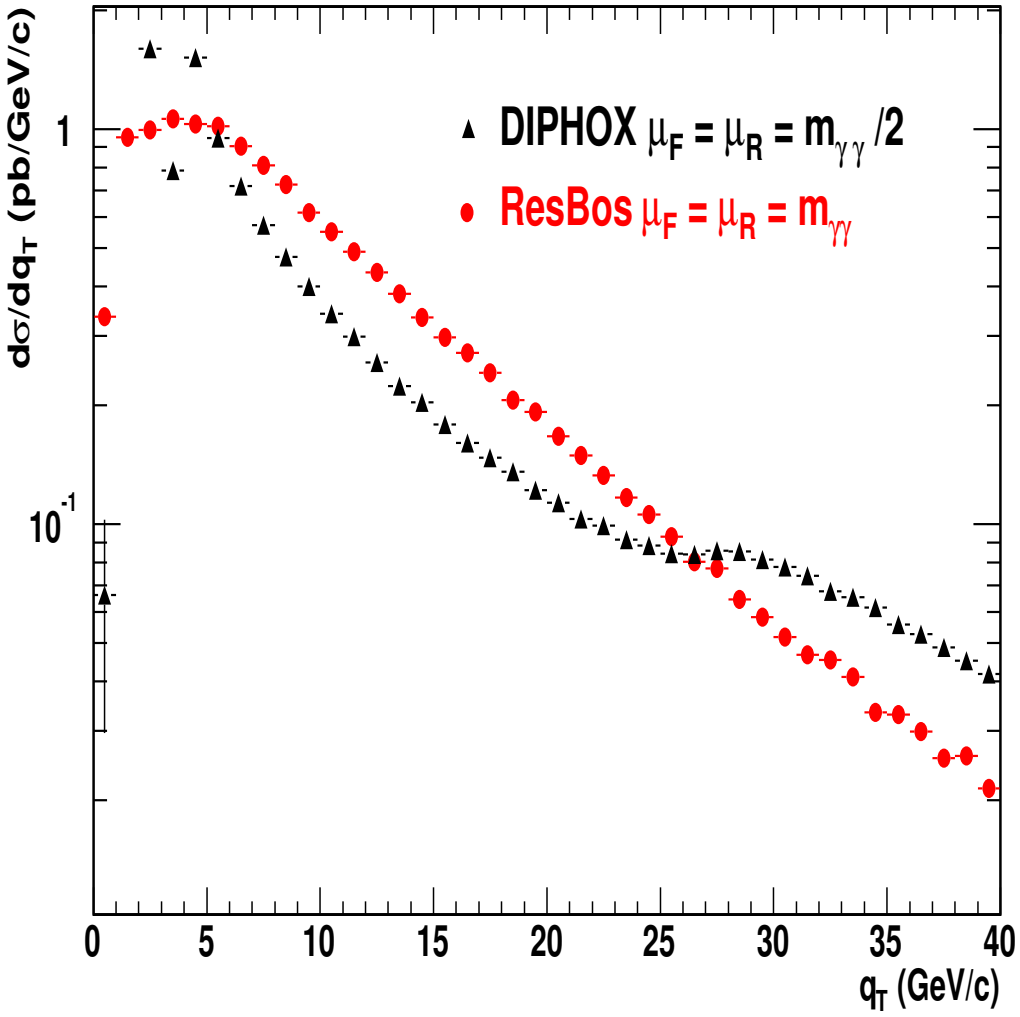

Figure 13: Diphoton system P_T distributions from DIPHOX and ResBos.

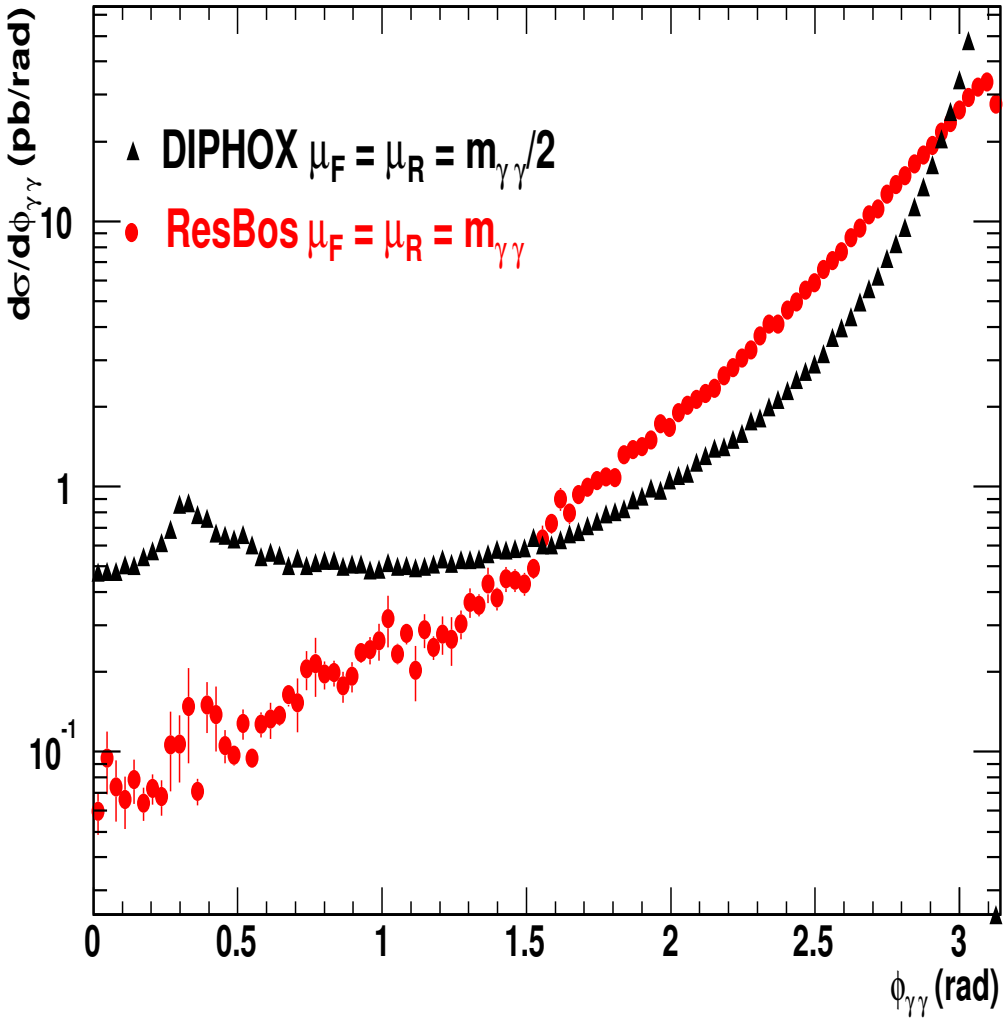

Figure 14: $\Delta\phi$ between the two photons from ResBos and DIPHOX.

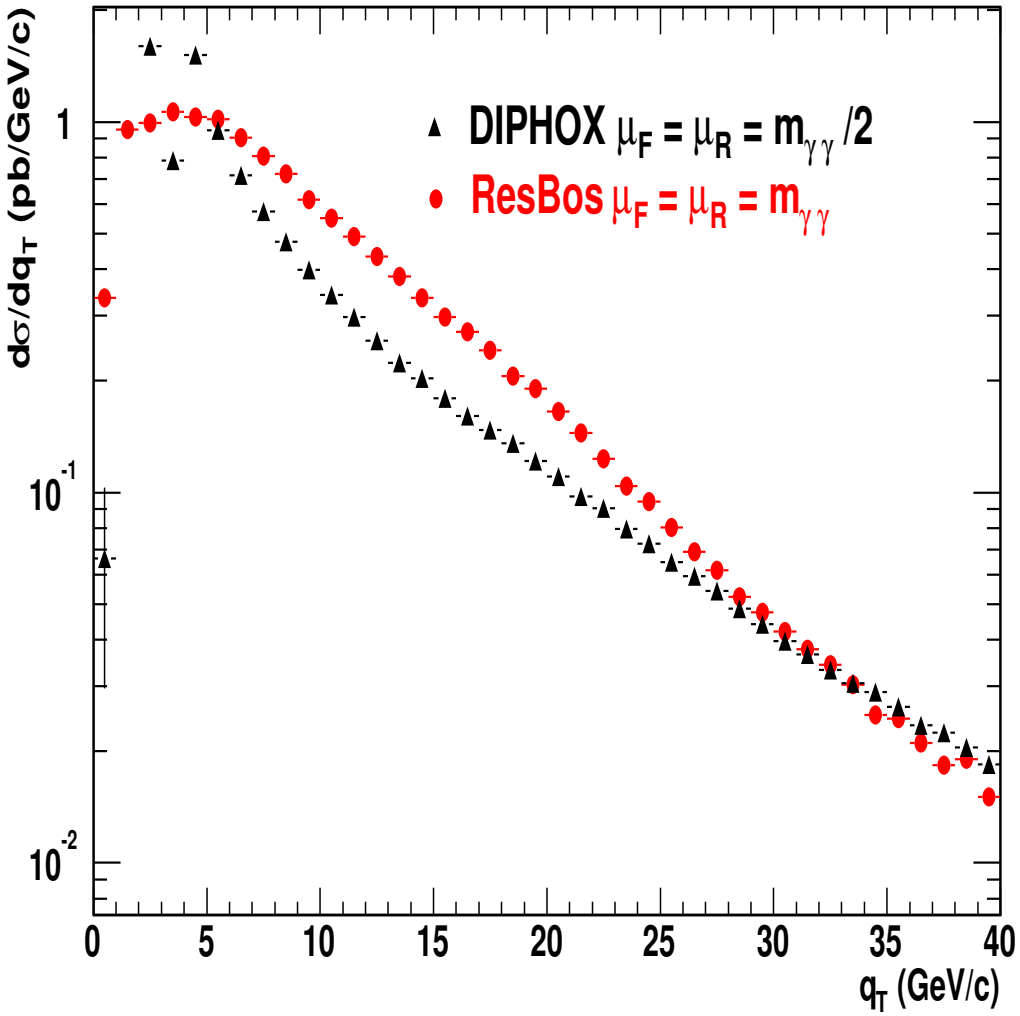

Figure 15: The q_T distribution from ResBos and DIPHOX, imposing the azimuthal angle cut : $\Delta\phi_{\gamma\gamma} > \pi/2$.

bin#	bin range (GeV)	mean m (GeV)	bin content (pb/GeV)	sys error (%)	DIPHOX (pb/GeV)	ResBos (pb/GeV)	Pythia (pb/GeV)
1	10-25	14.64	0.035±0.031	25	0.032	0.014	0.008
2	25-30	28.36	0.482±0.147	26	0.289	0.307	0.175
3	30-35	33.01	0.667±0.185	26	0.628	0.654	0.376
4	35-45	39.20	0.504±0.108	30	0.428	0.432	0.238
5	45-60	52.03	0.172±0.055	27	0.176	0.163	0.089
6	60-100	93.71	0.008±0.019	78	0.041	0.035	0.021

Table 4: comparison of the cross section vs. diphoton mass from data, DIPHOX, ResBos and Pythia. All predictions are binned in the same way as the data.

bin#	bin range (GeV)	mean qT (GeV)	bin content (pb/GeV)	sys error (%)	DIPHOX (pb/GeV)	ResBos (pb/GeV)	Pythia (pb/GeV)
1	0-1	0.5	0.764±0.326	19	0.066	0.335	0.533
2	1-2	1.5	1.283±0.469	23	2.938	0.954	1.151
3	2-4	3.02	1.015±0.383	29	1.191	1.028	0.938
4	4-8	5.82	1.043±0.246	32	0.938	0.941	0.457
5	8-12	9.82	0.281±0.226	44	0.378	0.594	0.211
6	12-16	13.64	0.443±0.157	27	0.216	0.362	0.121
7	16-24	18.78	0.196±0.093	26	0.122	0.185	0.070
8	24-32	26.93	0.128±0.065	23	0.083	0.072	0.032
9	32-40	35.48	0.107±0.050	48	0.055	0.032	0.013

Table 5: comparison of the cross section vs. diphoton qT from data, DIPHOX, ResBos and Pythia. All predictions are binned in the same way as the data.

bin#	bin range (π)	mean $\Delta\Phi$ (rad)	bin content (pb/rad)	sys error (%)	DIPHOX (pb/rad)	ResBos (pb/rad)	Pythia (pb/rad)
1	0-0.2	0.465	1.164±0.570	32	0.624	0.099	0.018
2	0.2-0.4	0.946	0.981±0.568	35	0.512	0.225	0.089
3	0.4-0.6	1.571	0.545±0.687	38	0.654	0.727	0.439
4	0.6-0.8	2.299	3.630±1.199	30	1.640	3.076	1.090
5	0.8-1.0	2.966	16.677±2.799	30	19.283	17.516	10.675

Table 6: comparison of the cross section vs. diphoton $\Delta\Phi$ from data, DIPHOX, ResBos and Pythia. All predictions are binned in the same way as the data.

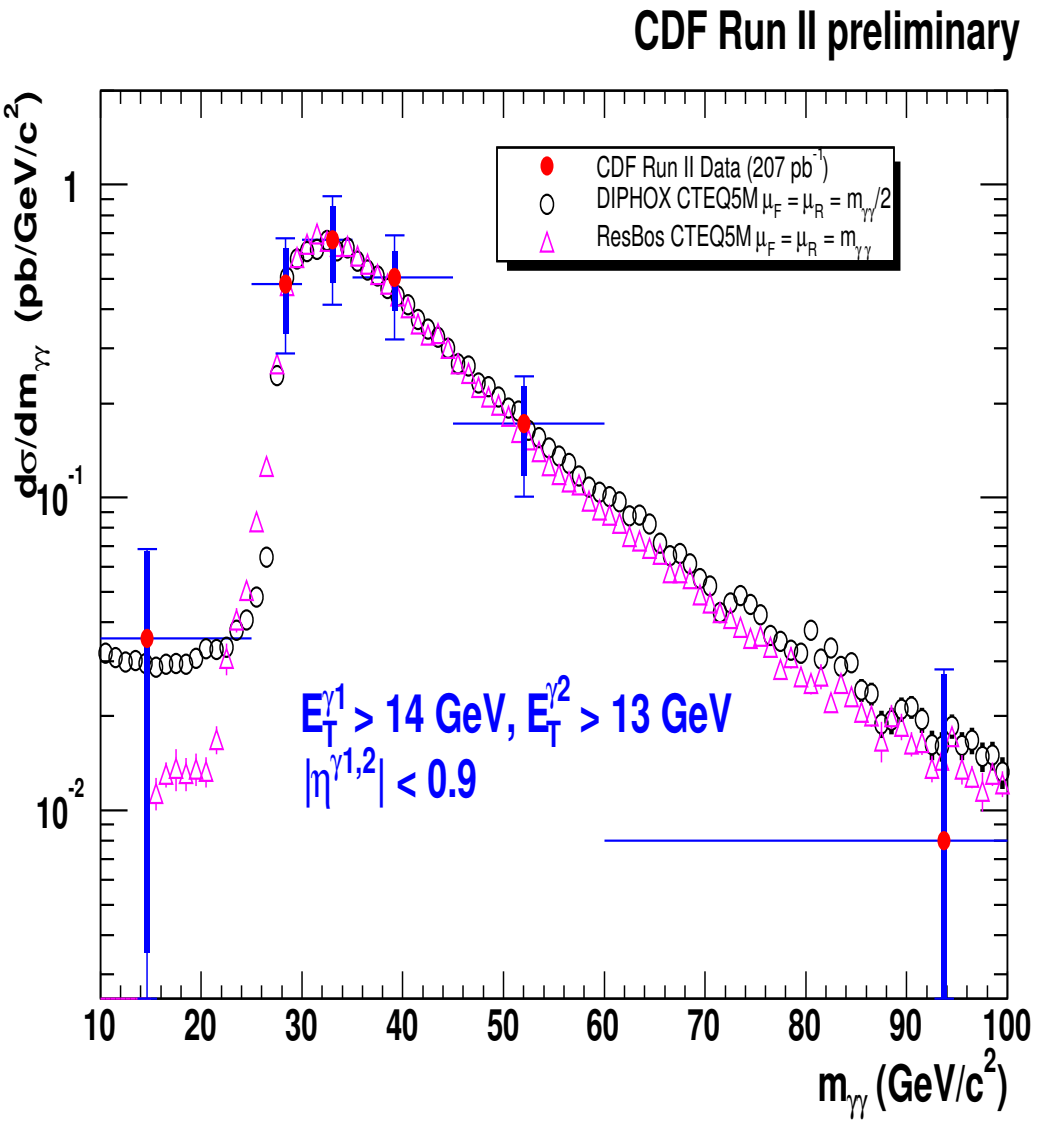

Figure 16: diphoton mass from DIPHOX, ResBos and CDF Run II data.

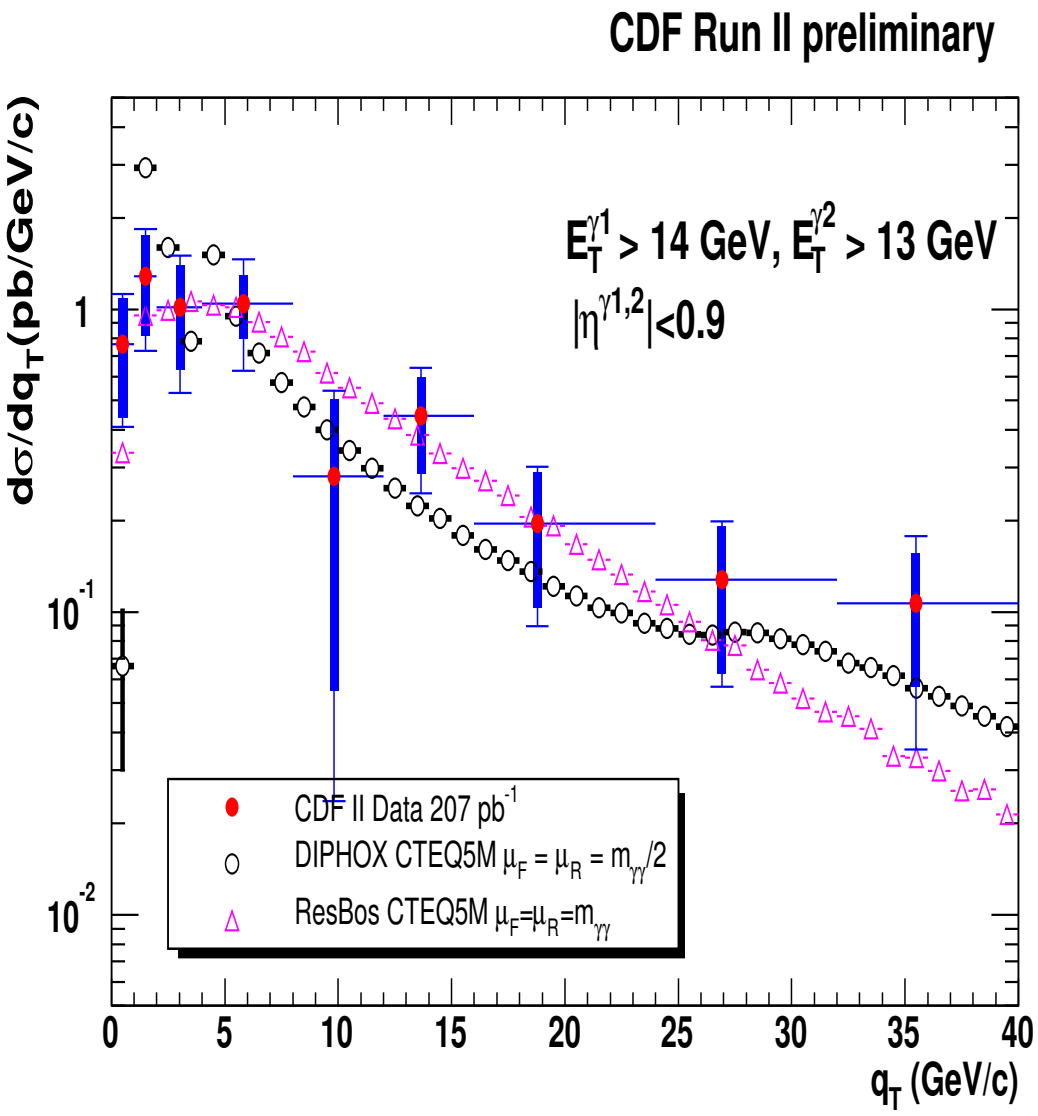

Figure 17: diphoton system P_T from DIPHOX, ResBos and CDF Run II data.

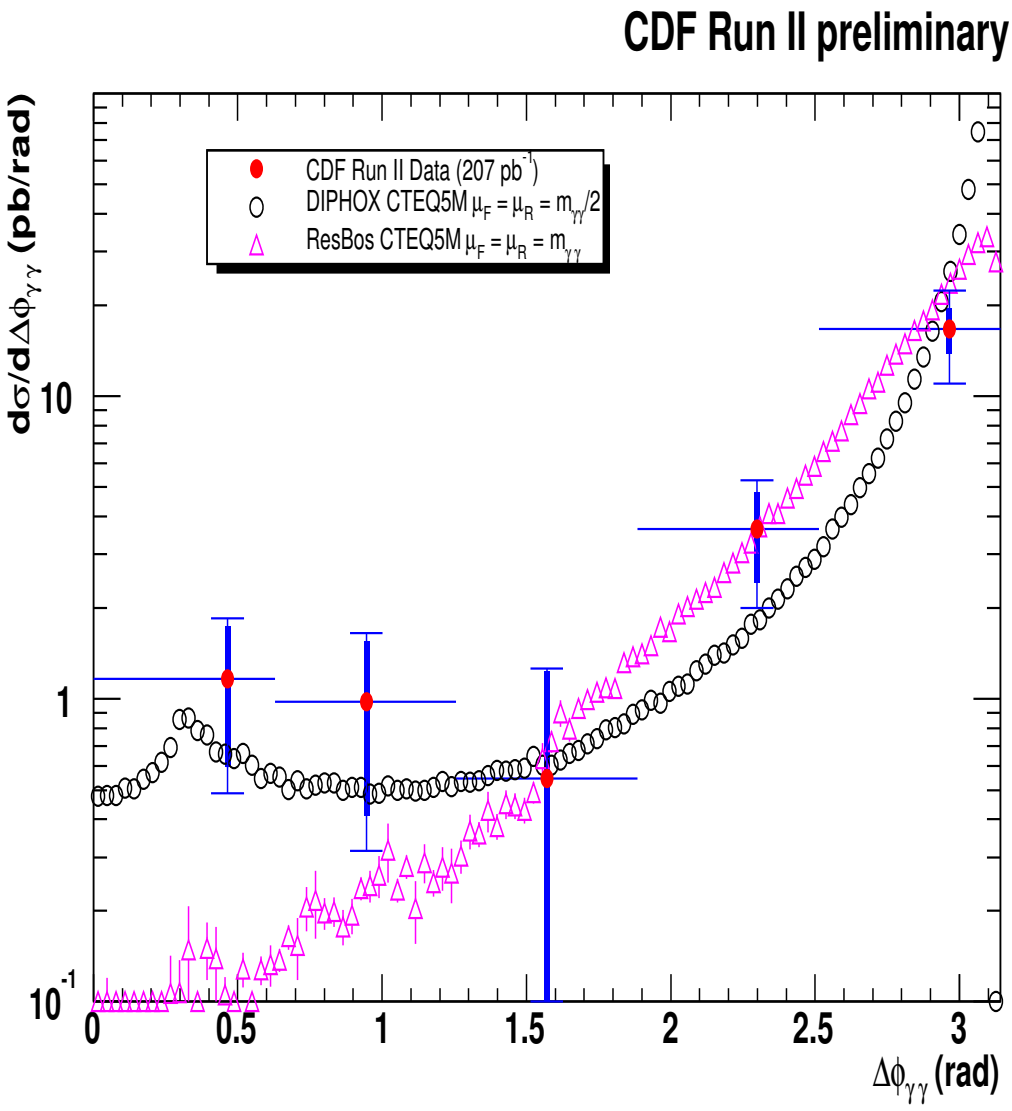

Figure 18: $\Delta\Phi$ between the two photons from DIPHOX, ResBos and CDF Run II data.

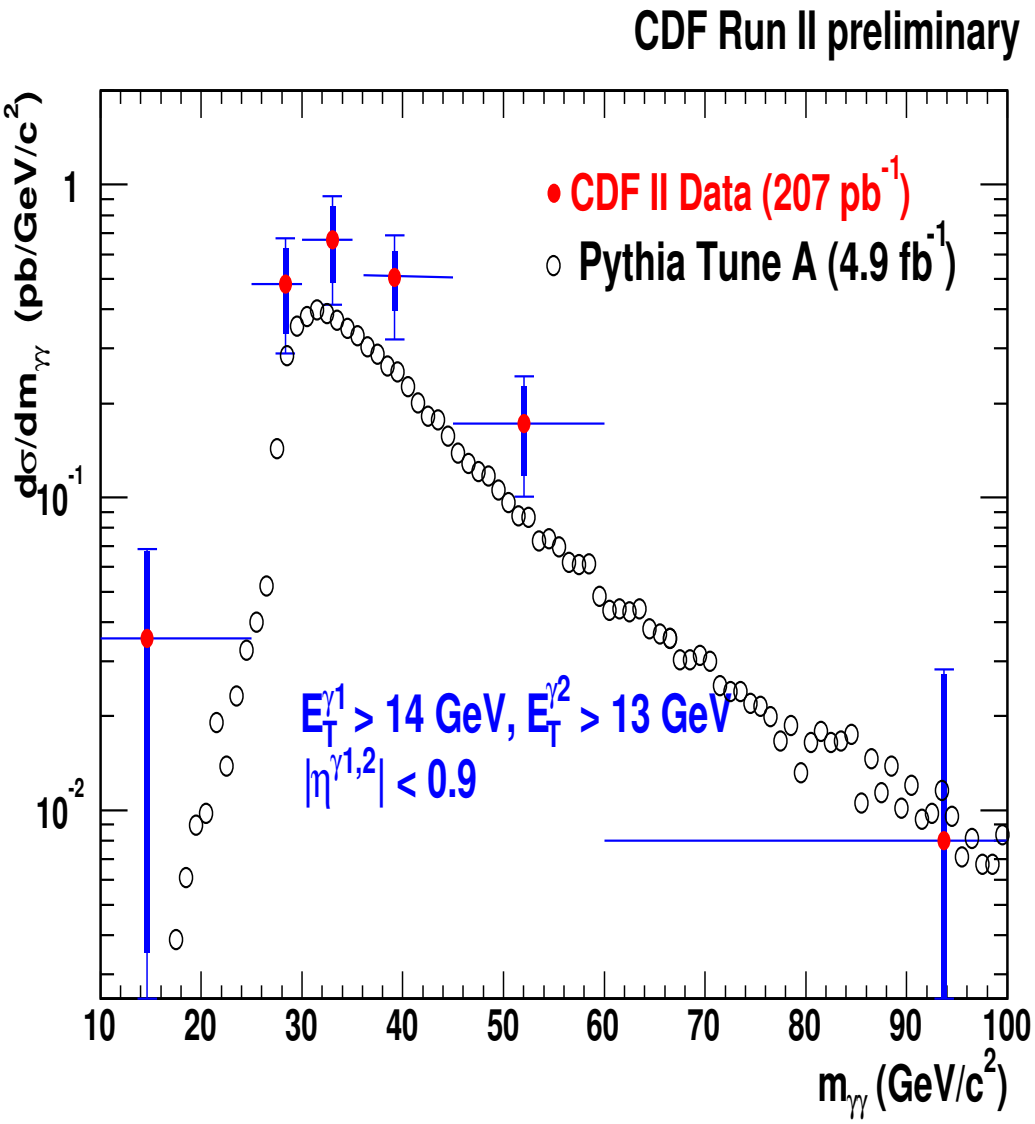

Figure 19: compare Pythia MC with data on the mass distribution.

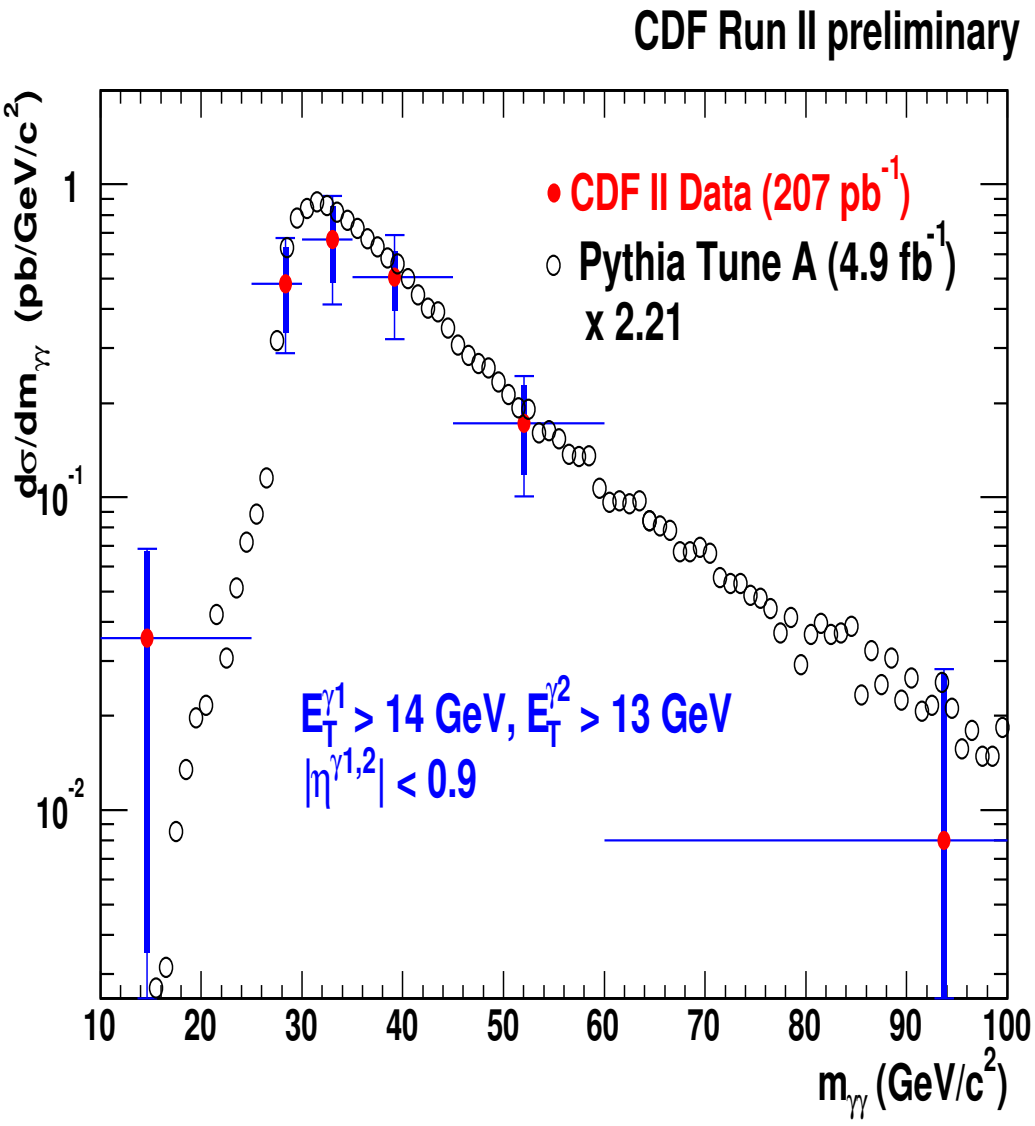

Figure 20: compare Pythia MC with data on the mass distribution, with the Pythia curve scaled up by a factor of 2.21.

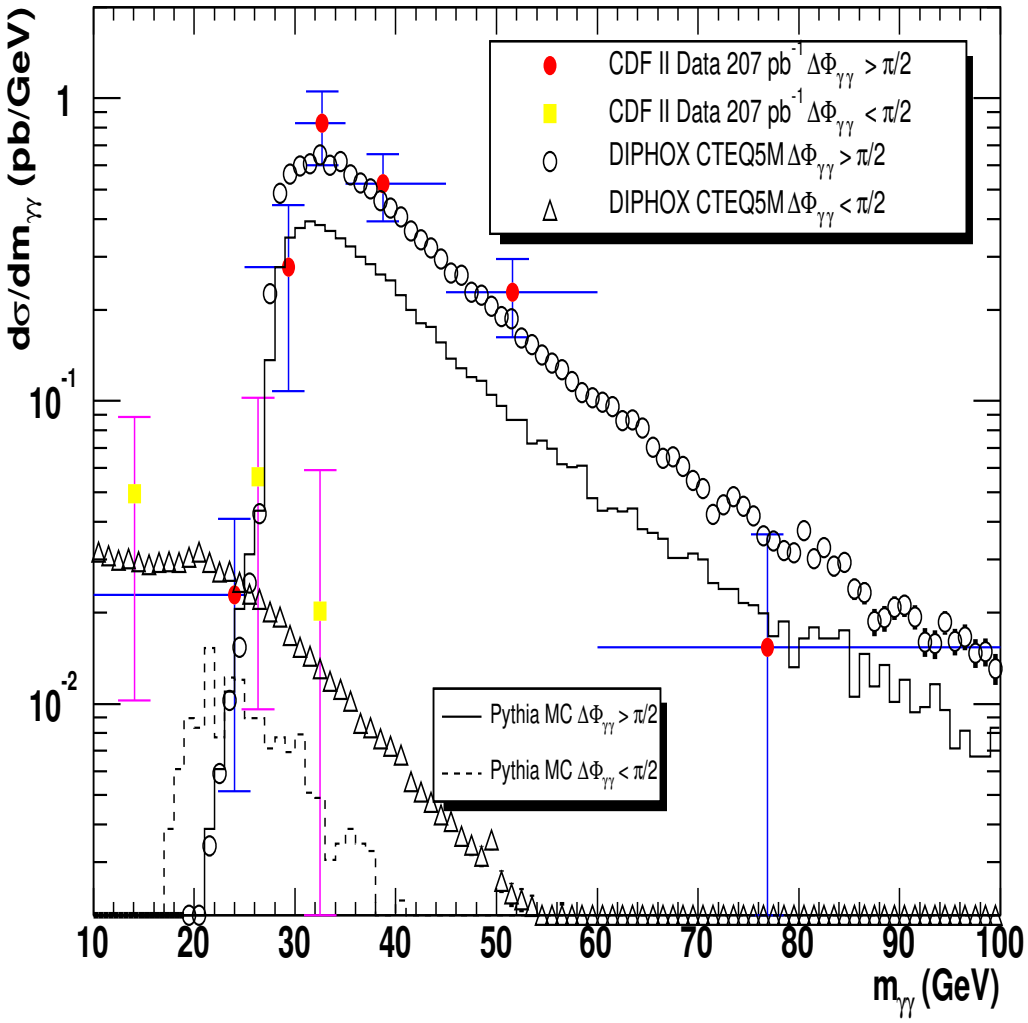

Figure 21: Compare the mass distributions separating $\Delta\Phi > \pi/2$ and $\Delta\Phi < \pi/2$. Error bars indicate stat. error only. The horizontal lines show the bin sizes of data points. Data from $\Delta\Phi > \pi/2$ and $\Delta\Phi < \pi/2$ binned in the same way.

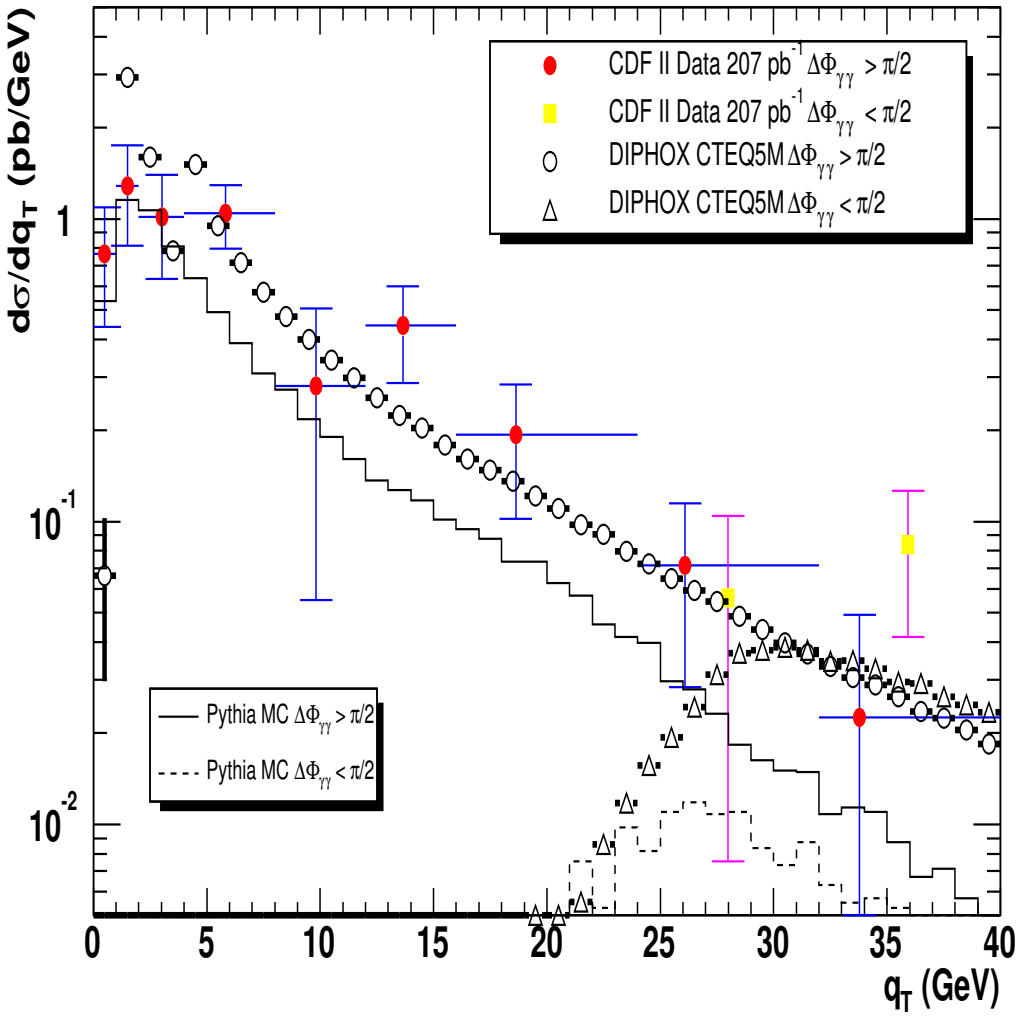

Figure 22: Compare the q_T distributions separating $\Delta\Phi > \pi/2$ and $\Delta\Phi < \pi/2$. Error bars indicate stat. error only. The horizontal lines show the bin sizes of data points. Data from $\Delta\Phi > \pi/2$ and $\Delta\Phi < \pi/2$ binned in the same way.

Talking about fragmentations, the variable z (defined as $P_T^{\gamma 2}/P_T^{\gamma 1}$, where $\gamma 1$ is the photon with higher P_T) is interesting. Consider the 2→2 process gq→ γq, with the quark in the final state fragments to a photon. This contribution is of order α_{em}^2. By transverse momentum conservation, $P_T^{\gamma 1}$ is equal to P_T of the quark in final state. The ratio $P_T^{\gamma 2}/P_T^{\gamma 1}$ is then just the variable z in the fragmentation function. In Fig. 28, we compare the distributions between data and DIPHOX, separating $\Delta\Phi > \pi/2$ and $\Delta\Phi < \pi/2$. There appears a peak in the DIPHOX prediction for $\Delta\Phi > \pi/2$ case. We verified the peak originates from one-fragmentation contribution. And it's primarily from the isolation criteria : the peak disappears if we remove the isolation cut in the calculation. See Fig. 24, 25, 26, and 27 in this note. It looks like the structure is created by the interplay between higher order effects and isolation criteria. The enormous peak at z=1 in Fig. 28 deviates from our observation in data. In Fig. **??**, it's shown that the soft gluon resummation in ResBos smears the peak and brings data and prediction to better agreement.

6 Conclusion

We have used 207 pb^{-1} of data to measure diphoton production rate. The results agree well with NLO QCD calculations.

7 ACKNOWLEDGMENT

We thank the Fermilab staff and the technical staffs of the participating institutions for their vital contributions. This work was supported by the U.S. Department of Energy and National Science Foundation; the Italian Istituto Nazionale di Fisica Nucleare; the Ministry of Education, Culture, Sports, Science and Technology of Japan; the Natural Sciences and Engineering Research Council of Canada; the National Science Council of the Republic of China; the Swiss National Science Foundation; the A.P. Sloan Foundation; the Bundesministerium fuer Bildung und Forschung, Germany; the Korean Science and Engineering Foundation and the Korean Research Foundation; the Particle Physics and Astronomy Research Council and the Royal Society, UK; the Russian Foundation for Basic Research; the Comision Interministerial de Ciencia y Tecnologia, Spain; in part by the European Community's Human Potential Programme under contract HPRN-CT-20002, Probe for New Physics; and by the Research Fund of Istanbul University Project No. 1755/21122001.

We thank the theorists on DIPHOX and ResBos: J.P Guillet, E. Pilon, Csaba Balazs, C-P Yuan for the invaluable discussions, and their providing and explaining the results of the calculations. The editor of this note is grateful for J.P Guillet's great patience and clear explanation on every stupid question he had about DIPHOX.

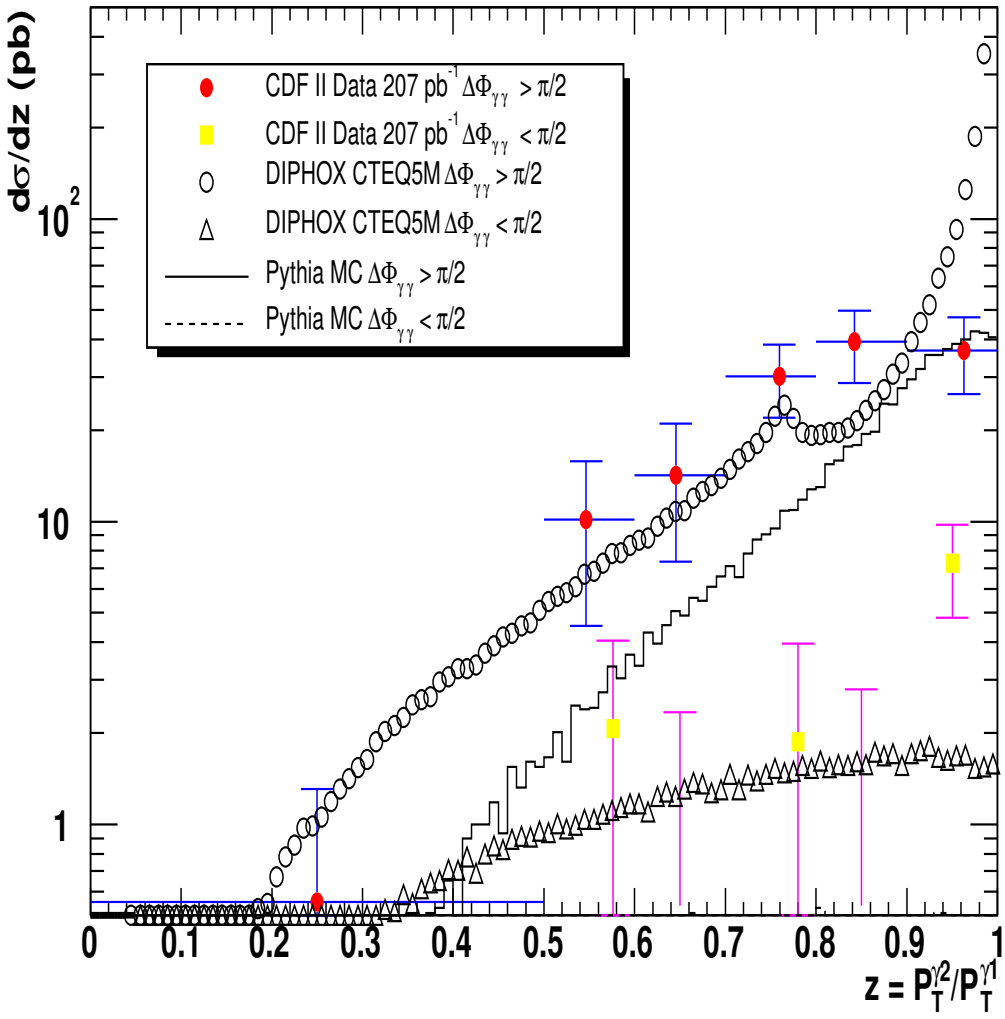

Figure 23: Compare the $z = P_T^{\gamma 2}/P_T^{\gamma 1}$ distributions separating $\Delta\Phi > \pi/2$ and $\Delta\Phi < \pi/2$. Error bars indicate stat. error only. The horizontal lines show the bin sizes of data theory. Data from $\Delta\Phi > \pi/2$ and $\Delta\Phi < \pi/2$ binned in the same way.

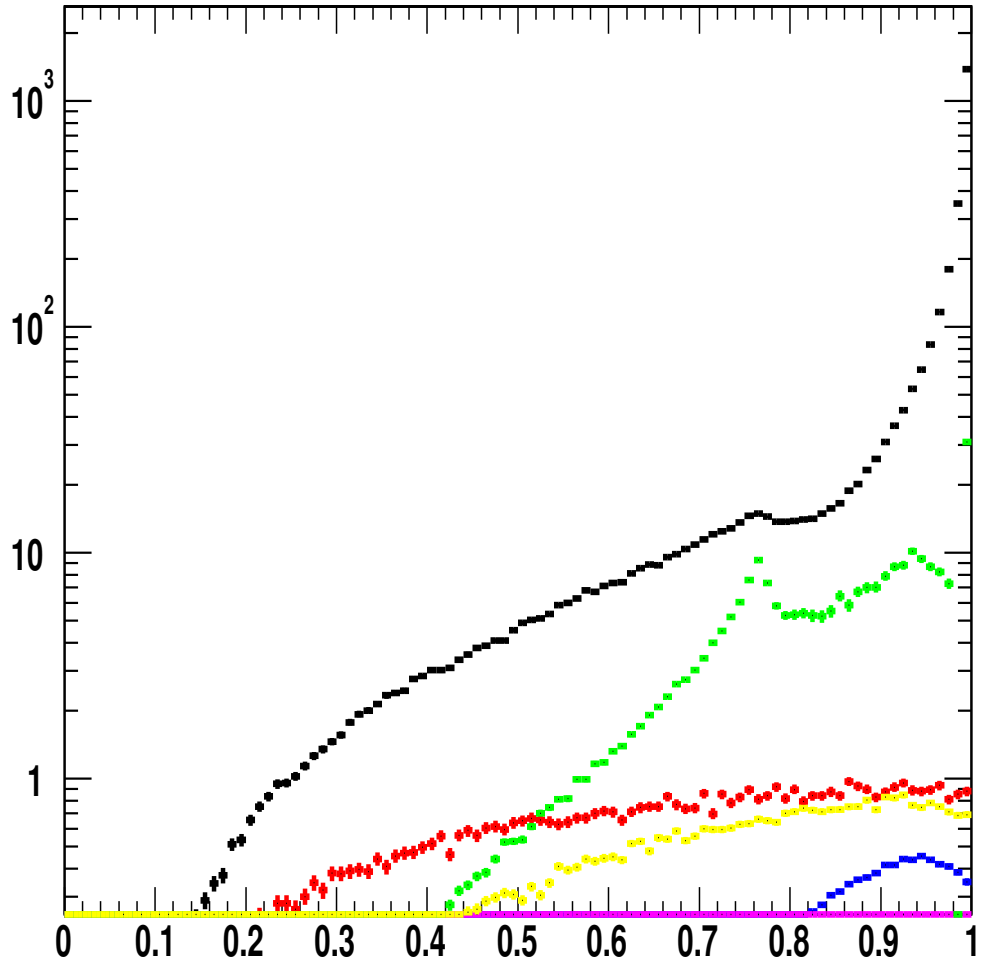

Figure 24: The $z = P_T^{\gamma 2}/P_T^{\gamma 1}$distribution from DIPHOX with isolation cut at 4 GeV, divided to 6 categories : black = two-direct $\Delta\Phi > \pi/2$, red = two-direct $\Delta\Phi < \pi/2$, green = one-frag $\Delta\Phi > \pi/2$, yellow = one-frag $\Delta\Phi < \pi/2$, blue = two-frag $\Delta\Phi > \pi/2$, magenta = two-frag $\Delta\Phi < \pi/2$. It's clear that the peak originates from one-frag contribution. The black curve has a bump at the same place, because the finite part of the collinear divergence of one-frag contribution is absorbed to two-direct.[12].

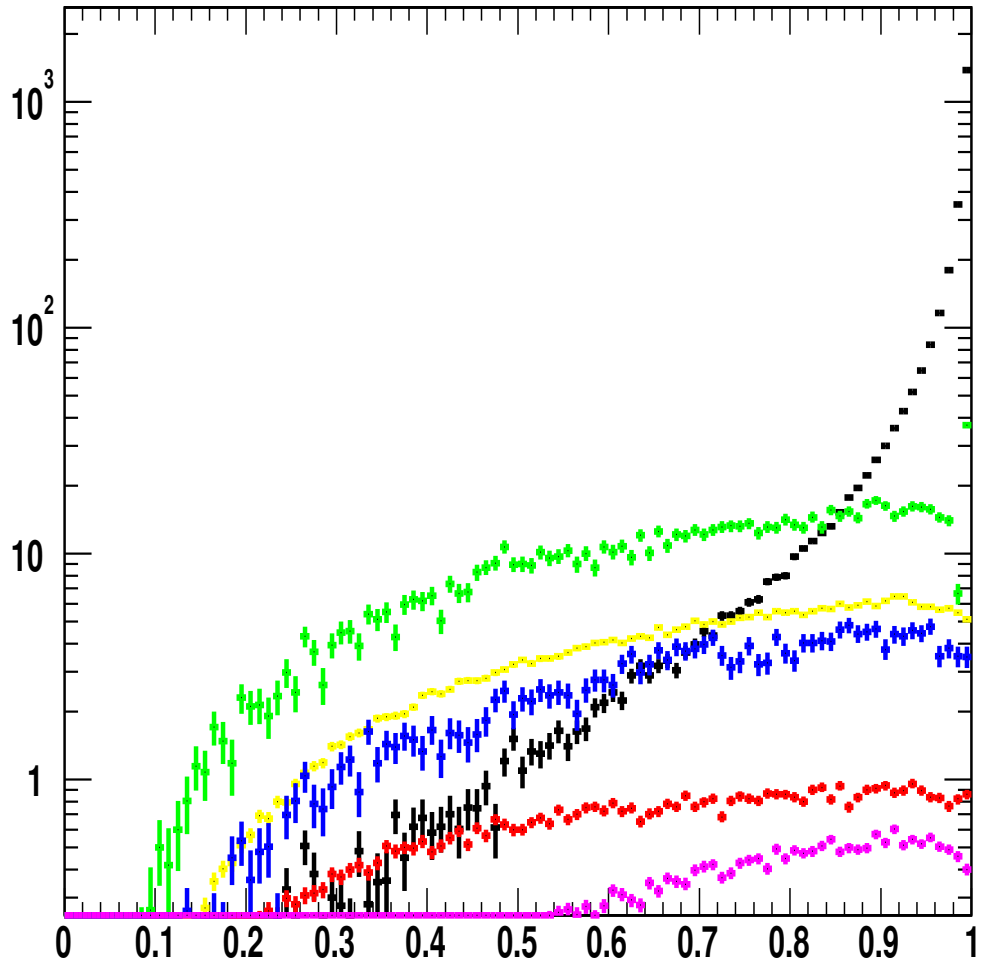

Figure 25: The $z = P_T^{\gamma 2}/P_T^{\gamma 1}$distribution from DIPHOX with no isolation cut. The color code is the same as in Fig. 24 : black = two-direct $\Delta\Phi > \pi/2$, red = two-direct $\Delta\Phi < \pi/2$, green = one-frag $\Delta\Phi > \pi/2$, yellow = one-frag $\Delta\Phi < \pi/2$, blue = two-frag $\Delta\Phi > \pi/2$, magenta = two-frag $\Delta\Phi < \pi/2$. The fragmentation contributions increase a lot with the removal of isolation cut. The peak on the green curve disappears.

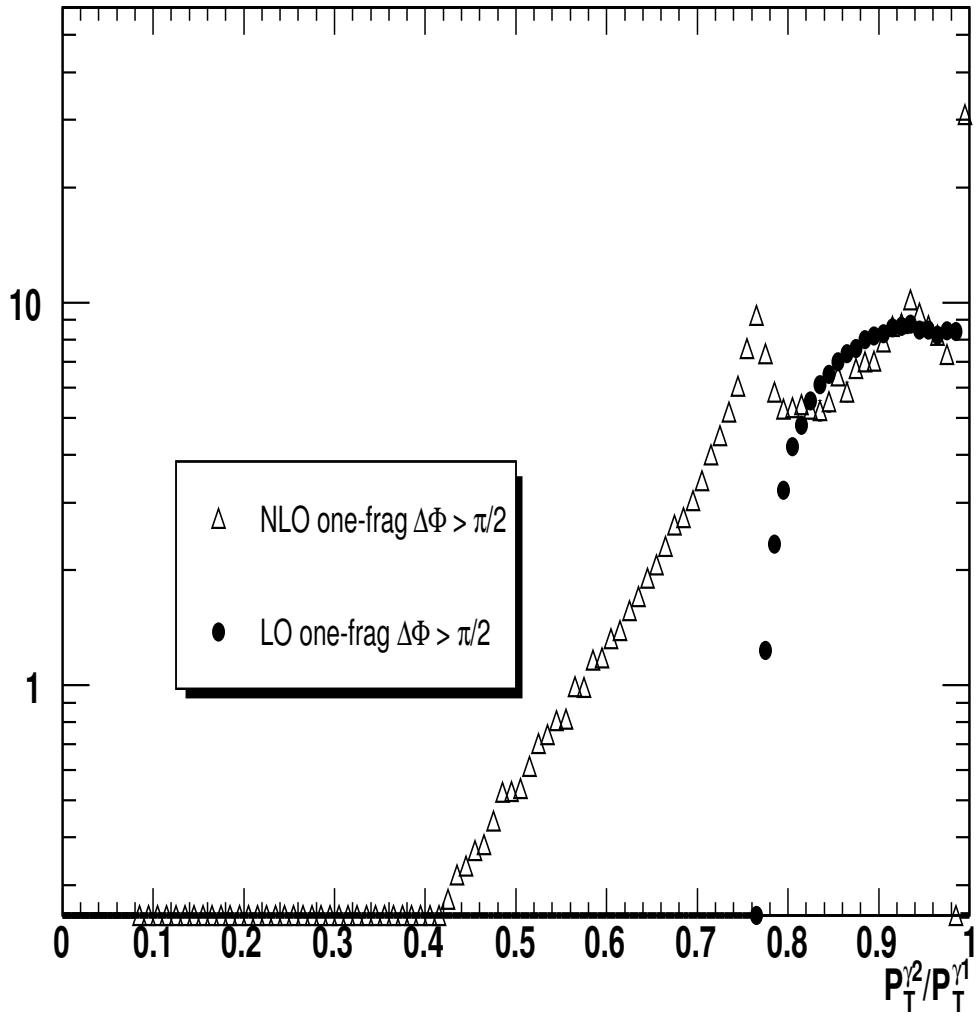

Figure 26: Shown is the one-frag $\Delta\Phi > \pi/2$ contribution with isolation cut (Green curve in Fig. 24) at LO and NLO separately.

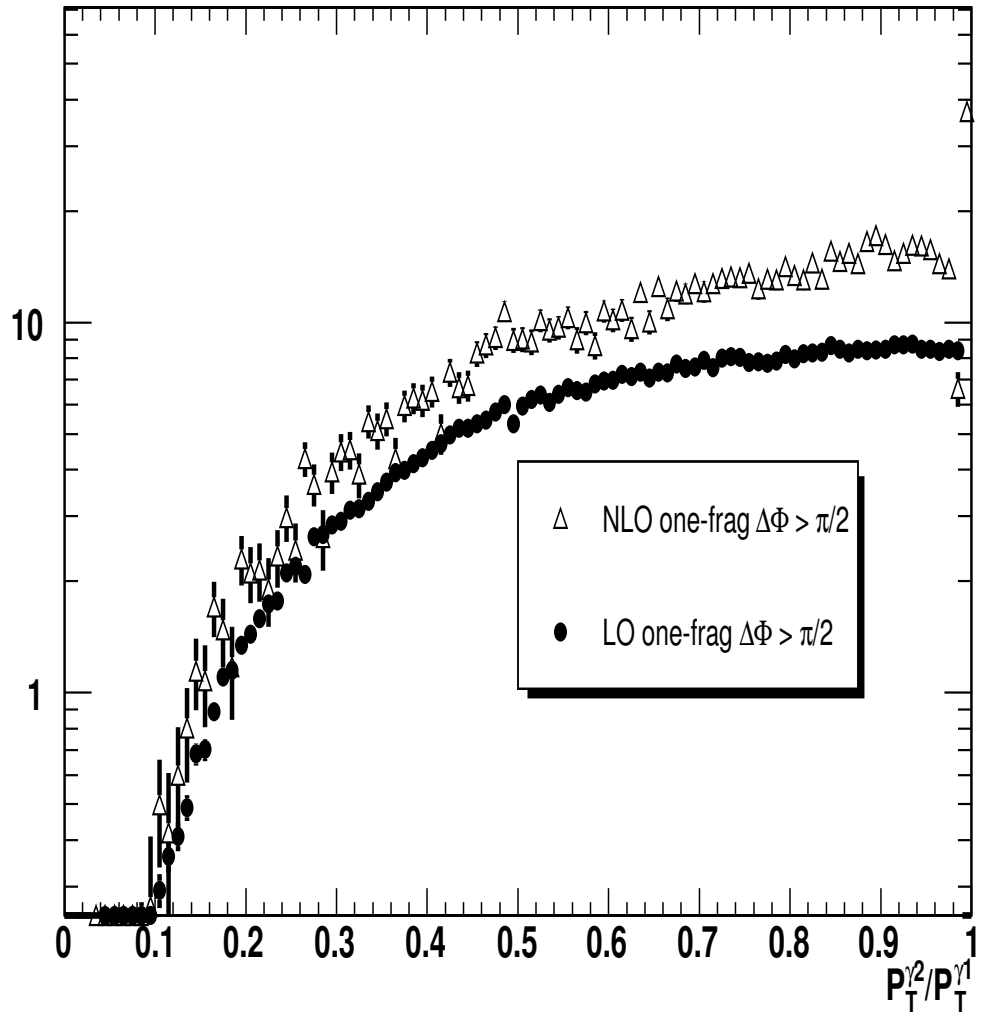

Figure 27: Shown is the one-frag $\Delta\Phi > \pi/2$ contribution without isolation cut (Green curve in Fig. 25) at LO and NLO separately.

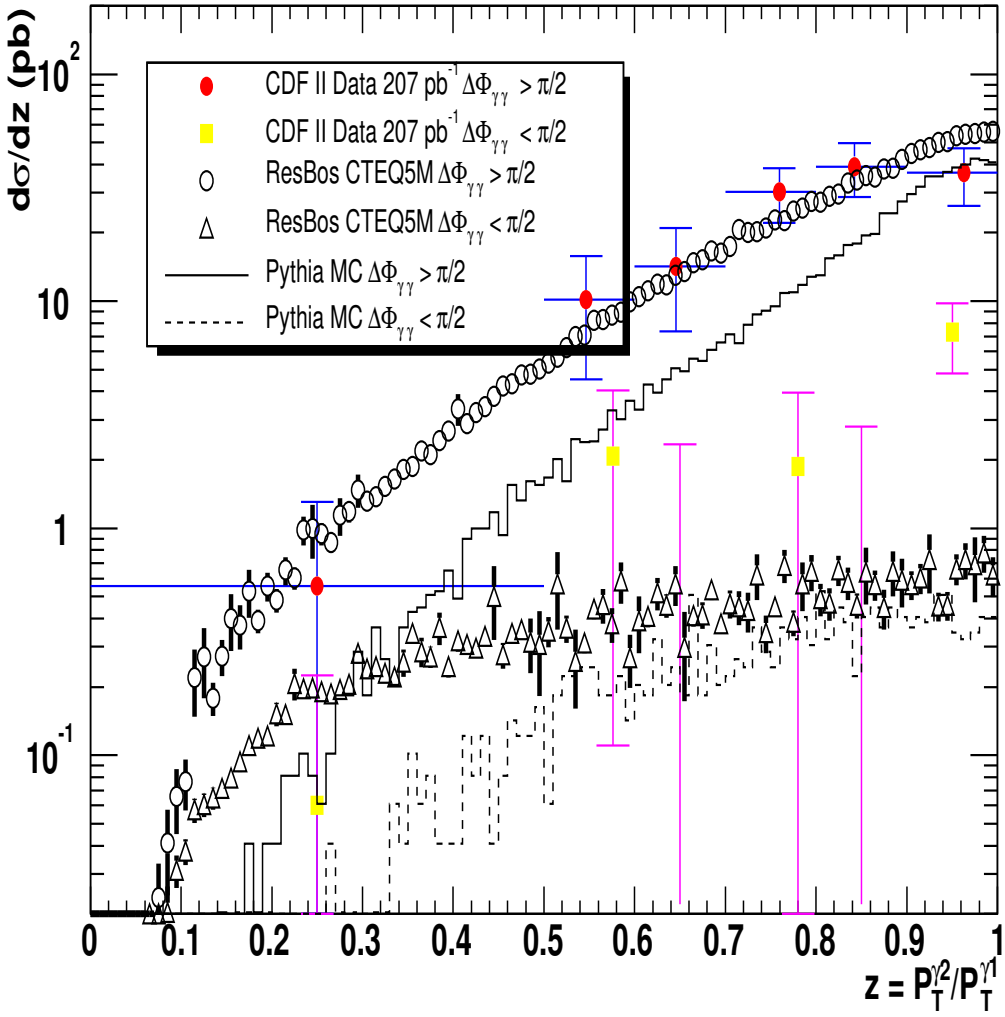

Figure 28: Compare the $z = P_T^{\gamma 2}/P_T^{\gamma 1}$ distributions from data and ResBos separating $\Delta\Phi > \pi/2$ and $\Delta\Phi < \pi/2$. Error bars indicate stat. error only. The horizontal lines show the bin sizes of data theory. Data from $\Delta\Phi > \pi/2$ and $\Delta\Phi < \pi/2$ binned in the same way.

References

[1] FERMILAB-Pub-96/390-E *The CDF II Detector Technical Design Report* Chap 12, the CDF II collaboration.

[2] CDF Note 2045 *Trigger tower organization and summing in $\eta - \phi$ space for Run II and beyond.* H.J.Frisch, M.Shochet,G.Sullivan,P.J.Wilson.

[3] CDF Note 5172 *Diphoton Production in 1.8TeV Proton-Antiproton Collisions*, Takeshi Takano

[4] CDF Note 5788 *L2 Isolation trigger information*,Bob Blair, John Dawson, William Haberichter, Steve Kuhlmann,Monica Tecchio

[5] Physics Review D volume 48,Page 2998, 1 October 1993. *prompt photon cross section measurement in $\bar{p}p$ collisions at $\sqrt{s} = 1.8$ TeV*, F.Abe et al (CDF collaboration)

[6] CDF Run II Photon background subtraction constants calibration and validation. *http://www-cdf.fnal.gov/internal/people/links/YanwenLiu/cescpr.html A separated CDF Note in preparation.*

[7] CDF Note 6601 *Update of the V+γ Analysis for Summer 2003*, Doug Benjamin, Alfred Goshaw, Michael Kirby, Helen Hayward, Beate Heinemann, Naho Tanimoto, Steve Errede.

[8] CDF Note 6331 *Event $|Zvtx| < 60$ cm Cut Efficiency for Run II*, W.K. Sakumoto and A. Hocker

[9] CDF Note 6101 *CPR Material counts for CDF Run II*, Minsuk Kim(Kyungpook National Univ), Ray Culbertson(Fermi National Lab), Robert Blair(Argonne National Lab).

[10] Eur.Phys.J. C 16,311-330(2000) *A full next-to-leading order study of direct photon pair production in hadronic collisions.* , T.Binoth, J.Ph.Guillet, E.Pilon, M.Werlen.

[11] JHEP 9710:005(1997), S.Catan and B. Webber.

[12] Jean-Philippe Guillet, private communications.

[13] Phys.Rev.D57:6934-6947,1998. [hep-ph/9712471] *Photon pair production with soft gluon resummation in hadronic interactions.* C. Balazs, E.L. Berger, S. Mrenna, C.P. Yuan. More information at Csaba's www site : http://www.pa.msu.edu/%7Ebalazs/ResBos/

[14] Phys. Rev. D63 (2001) 114016 T.Binoth, J.Ph.Guillet, E.Pilon and M.Werlen.